Water uptake of subpollen aerosol particles: hygroscopic growth, CCN activation, and liquid-liquid phase separation

Eugene F. Mikhailov[1,2], Mira L. Pöhlker[1], Kathrin Reinmuth-Selzle[1], Sergey S. Vlasenko[2], Ovid. O. Krüger[1], Janine Fröhlich-Nowoisky[1], Christopher Pöhlker[1], Olga A. Ivanova[2], Alexey A. Kiselev[3], Leslie A. Kremper[1], and Ulrich Pöschl[1]

[1]Multiphase Chemistry and Biogeochemistry Departments, Max Planck Institute for Chemistry, 55020   Mainz, Germany
[2]St. Petersburg State University, 7/9 Universitetskaya nab, St. Petersburg, 199034, Russia
[3]Atmospheric Aerosol Research Department, Institute for Meteorology and Climate Research, Karlsruhe Institute of Technology (KIT), Hermann-von-Helmholtz Platz 1, 76344 Eggenstein-Leopoldshafen, Germany.

Correspondence: Eugene F. Mikhailov (eugene.mikhailov@spbu.ru)

Abstract

Pollen grains emitted from vegetation can release subpollen particles (SPP) that contribute to the fine fraction of atmospheric aerosols and may act as cloud condensation nuclei (CCN), ice nuclei (IN), or aeroallergens. Here, we investigate and characterize the hygroscopic growth and CCN activation of birch, pine, and rapeseed SPP. A high humidity tandem differential mobility analyzer (HHTDMA) was used to measure particle restructuring and water uptake over a wide range of relative humidity (RH) from 2 % to 99.5 %, and a continuous flow CCN counter was used for size-resolved measurements of CCN activation at supersaturations (S) in the range of 0.2 % to 1.2 %. For both, subsaturated and supersaturated conditions, effective hygroscopicity parameters κ, were obtained by Köhler model calculations. Gravimetric and chemical analyses, electron microscopy, and dynamic light scattering measurements were performed to characterize further properties of SPP from aqueous pollen extracts such as chemical composition (starch, proteins, DNA, and inorganic ions) and the hydrodynamic size distribution of water-insoluble material. All investigated SPP samples exhibited a sharp increases of water uptake and κ above ~95 % RH, suggesting a liquid-liquid phase separation (LLPS). The HHTDMA measurements at RH> 95% enable closure between the CCN activation at water vapor supersaturation and hygroscopic growth at subsaturated conditions, which is often not achieved when HTDMA measurements are performed at lower RH where the water uptake and effective hygroscopicity may be limited by the effects of LLPS. Such effects may be important not only for closure between hygroscopic growth and CCN activation but also for the chemical reactivity, allergenic potential, and related health effects of SPP.

1 Introduction

The hygroscopic properties of atmospheric aerosols and their ability to act as cloud condensation nuclei forming cloud droplets are crutial for the radiative budget of the Earth's atmosphere (Hänel, 1976; Rader and McMurry, 1986; Pöschl, 2005; McFiggans et al., 2006; Andreae and Rosenfeld, 2008;

Swietlicki et al., 2008; Cheng et al., 2008; Zieger et al., 2013; Rastak et al., 2014, and references therein). The primary parameters, which determine the optical properties, CCN activity, reactivity, and deposition of aerosol particles are their size and composition. Depending on their sources and atmospheric processing (interaction with radiation, gases, and clouds), atmospheric particles consist of a complex mixture of organic and inorganic chemical components.

Primary biological aerosols (PBA) are a subset of atmospheric particles, which are directly released from the biosphere into the atmosphere. They comprise viable or dead cells, reproductive units, and fragments of organisms (bacteria, fungal spores, viruses, pollen, plant debris, etc.) (Després et al, 2012; Fröhlich-Nowoisky et al., 2016). PBA particles span the entire range of atmospheric aerosol particle diameters from nanometers to ∼100 μm, whereby the lower limit is given by the size of molecular clusters or macromolecules and the upper limit is related to rapid sedimentation. The number and mass concentrations of PBA particles over vegetated regions are typically on the order of 10^4 m^{-3} and 1 μg m^{-3}, respectively and account for around 30% in urban and rural air (Després et al, 2012; Fröhlich-Nowoisky et al., 2016). Laboratory experiments have shown that primary bioparticles are efficient CCN and IN and thus are assumed to influence the formation of cloud systems and precipitation (Möhler et al., 2007, Pöschl et al., 2010, Morris et al., 2014; Hoose and Möhler, 2012). Intense precipitation, in turn, can increase the concentrations of IN active bioaerosols in certain ecosystems (Huffman et al., 2013; Prenni et al., 2013). The positive feedback between the concentration of biological aerosol and precipitation is called *bioprecipitation* (Morris et al., 2014). It has been suggested that rainforests such as the Amazon Basin can act as biogeochemical reactors in which the precipitation induced by PBA materials sustain the production of plants, and hence PBA material, within the ecosystem (Pöschl et al., 2010).

Pollen is a category of bioaerosols that may spread in large quantities. It is the male gametophyte of gymnosperms and angiosperms. Pollen size ranges from 15 μm to 100 μm; its shape, when dry, is generally oval or spherical. The typical ambient number concentration of the pollen is estimated to be 10-10^3 m^{-3} (Després et al., 2012). In the Northern Hemisphere forests during strong pollination events pollen concentration may exceeds 10^4 m^{-3} (Williams and Després, 2017). Anemophilous (wind-driven) pollen despite their large size can undergo long distance dispersal up to ∼ 10^3 km (Sofiev et al., 2006; Kuparinen et al., 2009).

Water uptake of whole pollen grains at subsaturated conditions was studied by Pope (2010) and Griffiths et al. (2012) using an electrodynamic balance (EDB), as well as by Tang et al. (2019) and Chen et al. (2019), utilized a commercial vapor sorption analyzer. It was found that mass hygroscopic growth of pollen grains can be approximated by the κ-Köhler equation (Petters and Kreidenweis, 2007). For six pollen species studied by EDB the κ values were in the range of 0.05-0.10 (assuming a dry pollen density of 1 g cm^{-3}). These values agree with the κ range of 0.034-0.061

and 0.036-0.048 reported by Tang et al. (2019) and Chen et al. (2019) based on gravimetric measurements of six and eleven pollen samples, respectively. The EDB measurements by Pope (2010) and Griffiths et al. (2012) were complemented by Environment Scanning Electron Microscopy (ESEM) analysis, which showed that at RH < 85% the pollen grains swell internally by capillary effect through the germ apertures (Diehl et al., 2001). At RH > 89 %, the wetting of the pollen surface was observed. The surface absorption of water was first detected at the pollen pore sites and proceeded to engulf the pollen grain as a whole. Pollen has been identified as a potential natural source of giant CCN (Griffiths et al., 2012). Many studies have reported a high IN activity of various pollen species and highlight their potential importance for mixed phase clouds in biologically-influenced environments (Diehl et al., 2001, 2002; von Blohn et al., 2005; Chen et al., 2008; Pummer et al., 2012). Although pollen grains are assumed to account only for a small fraction of IN active on a global scale, their local and regional impact on cloud microphysics could be substantial (Hoose et al., 2010).

In addition to the direct emission of intact pollen grains, the rupture of pollen and subsequent release of fine particles may contribute more substantially to ambient aerosol particle concentration. Fresh pollen grains can rupture at high humidity (Taylor et al., 2002, 2004) and during precipitation events (Grote et al., 2001, 2003; Hughes et al., 2020). They may also mechanically rupture under turbulent conditions by impact forces (Visez et al., 2015). When pollen grains rupture, they release cytoplasmic material known as subpollen particles (SPP) ranged from several nanometers to about 1 μm (Grote et al., 2003; Taylor et al., 2004). Rupture can occur on open anthers (i.e., at the surface), and SPP can be subsequently dispersed to the atmosphere by disturbances like wind in dry conditions (Taylor et al., 2004). Regional transport and weather patterns may facilitate the transport of these smaller particles and lead to longer atmospheric residence time (Wozniak et al., 2018; Hughes et al., 2020).

Augustin et al. (2013) and O'Sullivan et al. (2015) have shown that the nano-scale range SPP washed of pollen grains are IN active even with a molecular mass below 1000 kDa. Laboratory experiments with six fresh pollen samples revealed that SPP ranging 50-200 nm are CCN active in the supersaturation range of 0.81-0.12% (Steiner et al., 2015). Mikhailov et al. (2019) found an almost constant CCN-derived κ value of 0.12 to 0.13 for SPP produced by birch, pine, and rapeseed pollen grains. As shown below, these values are underestimated since they do not account for the irregular shape of the initial dry SPP. Wozniak et al. (2018) developed the first model of atmospheric pollen grain rupture and implemented the mechanism in regional climate model simulations over the spring pollen season in the United States with a CCN-dependent moisture scheme. They showed that in contrast to positive "bioprecipitation" feedback caused by IN active bioparticles (Morris et al., 2014), the CCN-active SPP suppress precipitation. Model calculations indicate that when the number of SPP

is equal to 10^6, the suppression effect in clean conditions is 32%, while their lower value (10^3) produces a negligible effect on precipitation.

Almost all angiosperm pollen grains are covered by a viscous material called *pollenkitt*, comprising saturated and unsaturated lipids, carotenoids, flavonoids, proteins, and carbohydrates (Piffanelli et al., 1998; Pacini and Hesse, 2005; Chichiriccò et al., 2019). The CCN properties of the submicron pollenkitt particles obtained from six different plant species were studied by Prisle et al. (2019). It was shown that some pollenkitt species are surface-active and therefore decrease surface tension. The CCN-derived κ values were generally between 0.1 and 0.2. For all species studied, the maximum κ was observed at activation diameters ranging between 50-70 nm and steeply decreased above ~70 nm. Prisle et al. (2019) suggested that this behavior reflects the impact of pollenkitt surface activity on CCN activation, which decreases with particle growth factor increasing.

To our knowledge, no hygroscopic properties of SPP in subsaturated conditions have been presented in literature. Similar to other atmospheric aerosol particles, the hygroscopicity of SPP influences their life cycle in the atmosphere and the related direct and indirect effects on radiation budget. In addition, SPP hygroscopicity is a key factor enhancing the allergenic potential of chemically modified pollen allergens, like proteins (Pöschl et al., 2015; Reinmuth-Selzle et al., 2017). It was documented that chemical modification of proteins by atmospheric nitrogen dioxide (NO_2) and ozone (O_3) proceeds efficiently at high RH within the particle bulk. The rate of the protein nitration and dimerization in the liquid phase occurred almost one order of magnitude higher in comparison to amorphous and semi-solid SPP states (Reinmuth-Selzle et al., 2014; Liu et al., 2017).

In this study, we investigated the hygroscopic properties and CCN activity of birch, pine and rapeseed SPP for water saturation ratios between 0.02 and 1.012. These investigations were complemented with different chemical analyses of the subpollen components. A separate HHTDMA experiment was performed to evaluate the size-dependent restructuring of aerosol particles to correct their hygroscopic growth and CCN activity. We also conducted gravimetrical measurements coupled with dynamic light scattering, which allowed estimating the effect of the colloid nanoparticles on the SPP hygroscopicity. Together with the experimental analysis the κ-Köhler model was applied to reconcile the hygroscopicity and cloud condensation activity of subpollen particles.

2 Material and methods

2.1 Sample preparation

Pollen samples were collected from common genera belonging to the deciduous, coniferous and herbaceous plants. These species are: birch pollen (*Betula pendula*), pine pollen (*Pinus silvestris*), and rapeseed (*Brassica napus*), respectively. The aqueous pollen extracts were prepared by placing ~200 mg of pollen grains in 100 ml MilliQ-water (2mg ml^{-1}). The solutions were then 40 min extracted in

an ultrasonic bath (frequency, 35 kHz; Bandelin, Sonorex Super 10P, Germany) in 1 min on /off intervals. The aqueous extracts were filtered through a 0.45 µm syringe filter device (25mm GD/X, sterile, 6901-2504, GE Healthcare Life Science, Whatman). The resulting filtered solution was atomized and dried to generate particles for HHTDMA and CCN measurements. The same extraction protocol was used for chemical and gravimetric analysis. It is expected that the aqueous extracts contain both surface substances (Suppl. S1) and cytoplasmic material released either due to osmotic shock or/and pollen rupture (Pummer et al., 2012; Steiner et al., 2015). As shown by Laurence (2011) the pollen degradation occurs more efficiently under sonification, therefore we used an ultrasonic bath.

2.2 Gravimetric analysis

Hereinafter we consider that the total solid (TS) in the filtered solution is the sum of both, the total dissolved species and total suspended solids (TSS) (hydrosols). The TS mass of subpollen species in the filtered solution was determined gravimetrically as follows. Aqueous pollen extracts were prepared as described in Sect. 2.1 with the exception that 100 mg of pollen grains were suspended in 50 ml MilliQ-water (2 mg ml^{-1}). After filtration the loaded syringe filter (25 mm, 0.45 µm) was first kept in a desiccator to gently remove liquid water and then dried in vacuum for 24 h (residual pressure 1 hPa). The weighing for the gravimetric PM determination was done with a microbalance (0.01 mg sensitivity) at 25°C and ~ 30 % RH, and the filters and impaction substrates were equilibrated at these conditions for 24 h prior to weighing. The TS was then determined as the difference between the initial pollen mass and the mass captured by the syringe filter (Suppl.S2, Table S.1). The mass ratio (*MR*) of the penetrated material through the filter to initial mass was further used to calculate the mass fraction (w_i) of chemical species: $w_i = C_i/MRC_0$, where C_i is the mass concentration of species (*i*) in the filtered solution and C_0 is the initial mass concentration of pollen grains in water, respectively. To determine C_i of the water-soluble species chemical analyses were performed as described below. The total mass concentration of suspended material was determined as $C_{TSS} = C_{TS} - \sum_i C_i$.

2.3 Scanning electron microscopy (SEM)

The samples were investigated with a high-resolution SEM (ZEISS Merlin). Operation conditions: 0.4 kV accelerating voltage, In-Lens detector of SE, 3.6 mm working distance. Particle samples were collected directly onto a 3mm TEM copper 300 mesh grids, coated with a 30–60 nm thick Formvar film.

2.4 Chemical analysis

2.4.1 Materials

The following chemical and materials were used in this study: Ultra pure water from a GenPur^{TM} UV-TOC/UFxCAD Plus water purification system (Thermo Scientific, Braunschweig, Germany), D-(+)-

Glucose (> 99,5%, catalog #G8270, Sigma Aldrich, USA), phenol (> 99%, catalog 33517, Sigma Aldrich, USA), sulfiric acid (98%, catalog #1120801000, Merck, Darmstadt, Germany), Qubit® Assay Tubes (clear 0.5ml PCR tubes, Q32856, Thermo Scientific, Braunschweig, Germany), Qubit™ Protein assay kit (Q33211, 0.25-5µg, Invitrogen, Thermo Fisher Scientific, Braunscheig, Germany), Qubit™ dsDNA HS assay kit (Q32854, 0.2-100ng, Invitrogen, Thermo Fisher Scientific, Braunschweig, Germany), protein LoBind tubes (100 safe-lock tubes, PCR clean, 0030108132, Eppendorf, Hamburg, Germany), starch assay kit (SA20, Sigma Aldrich, USA).

2.4.2 Carbohydrate analysis

According to the protocol by Masuko et al. (2005) D-(+)-Glucose standard solutions were prepared in pure water at different concentrations (50, 250, 500, 1000, 2000, 3000 µM). 2.5 % (w/v) phenol solution was prepared (0.25 g phenol in 5 ml pure water. 50 µl of the standard solution and of each sample were added to the 96 well-plate in triplicates. Immediately 30 µl of the phenol solution were added and the well plate was incubated for 5 min at 90 °C in a drying oven (Binder, Tuttlingen, Germany) of 490 nm using a microplate reader (Multiscan GO, Thermo Scientific, Braunschweig, Germany).

2.4.3 Starch analysis

Water-extractable starch

The assay was done according to the manufacture´s protocol (Starch Assy Kit, Sigma Aldrich). Briefly, 1 ml of each of the TS was added to 1 ml of the starch assay reagent containing 50 units/ml of amyloglucosidase, which is an enzyme catalyzing the hydrolysis of starch to glucose. In the second step, the mixture is added to the glucose assay reagent containing 1.5 mM nicotinamide adenine dinucleotide (NAD), 1.0 mM adenosine triphophosphate (ATP), 1.0 units/ml of hexokinase, and 1.0 unit/ml of glucose-6-phosphate dehydrogenase (G6PDH). The reaction of the assay involve the following steps:

$$\text{Starch} + (n-1)\ H_2O \xrightarrow{\text{Amyloglucosidase}} (n)\ \text{Glucose}$$

$$\text{Glucose} + \text{ATP} \xrightarrow{\text{Hexokinase}} \text{Glucose-6-Phosphate} + \text{ADP}$$

$$\text{G6P} + \text{NAD} \xrightarrow{\text{G6PDH}} \text{NADH} + \text{6-Phosphogluconate}$$
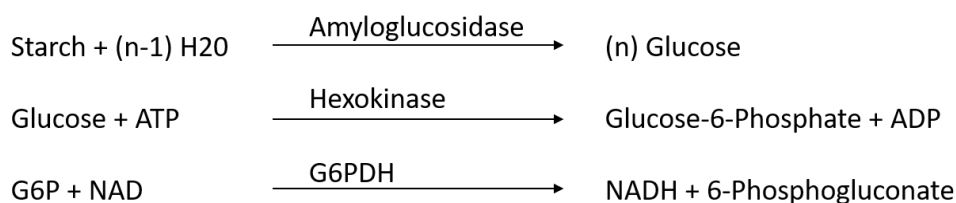
The increase in NADH (reduced form of NAD) and thus in the absorbance at 340 nm is directly proportional to the final glucose concentration.

Total starch (Resistant starch, extraction with DMSO)

The solid pollen samples were prepared as followed: 50µg of rapeseed, birch and pine pollen were dissolved in 10 ml dimethyl sulfoxide (DMSO) (1742589, Fisher scientific) and 2.5ml 8M hydrochloric acid and were incubated for 30 min at 60° C in an oven. After cooling down to room temperature, 25 ml of pure water was added and the pH was adjusted to approximately 5 with 5N sodium hydroxide solution. The samples were then treated as the water-extracted samples described above and the starch content was determined by the starch assay kit.

2.4.4 Protein analysis

The protein concentration of the birch, pine and rapeseed pollen extracts was determined using a Qubit® protein assay Kit according to the manufacturer's instruction (Thermo Fisher Scientific, Braunschweig, Germany). Briefly, 10µl of standard and samples are diluted in Qubit®Buffer to a final assay volume of 200µl. After vortexing for 2-3 seconds and incubation for 15 min at room temperature, the tubes were inserted in the Qubit® 3.0 fluorometer (Invitrogen, Thermo Fisher Scientific, Braunschweig Germany), and the samples and standards were measured in triplicates.

2.4.5 DNA analysis

The DNA concentration of aqueous pollen extracts was determined according to the manufacturer's instruction of the Qubit® dsDNA HS assay kit (Q32854, 0.2-100ng, Invitrogen, Thermo Fisher Scientific, Braunschweig, Germany).

2.4.6 Ion analysis.

Capillary electrophoresis system "CAPEL-105/105M" (Lumex,) is equipped with variable UV-spectrophotometric detector, with a wavelength range of 190–400 nm. The specialized software "Elforan" (Lumex, Russia) was used for instrument control and data acquiring. Fused-silica capillaries with external polyimide coating (Polymicro Technologies, Phoenix, AZ, USA), 50 µm, I.D., 360 µm, O.D., effective length of 50 cm and total length of 60 cm. Hydrodynamic sample injection: 1500 mbar×sec (30 mbar×50 sec).

2.5 Size-resolved cloud condensation nuclei (CCN) measurements

A detailed description of the operation of the CCN counter (CCNC) and the subsequent data analysis can be found in Pöhlker et al. (2016), which is the basis for the CCN part of this study. Briefly, size-resolved CCN measurements were conducted using a continuous-flow stream wise thermal-gradient CCN counter (model CCN-200, DMT, USA) coupled to a Differential Mobility Analyzer (DMA) (model 3081, TSI, DMA) and a condensation particle counter (CPC) (model 3772, TSI, USA). The CCNC was operated at a total flow rate of 0.5 l min^{-1} with a sheath-to-aerosol flow ratio of 10. The water vapor supersaturation (S) was regulated by the temperature difference of the CCNC flow column (ΔT) and calibrated using ammonium sulfate aerosol and activity parameterization Köhler model

(AP3) as described in Rose et al. (2008). Based on the calibration procedure, the overall uncertainty of S is estimated to be ~7 %. For each CCN measurement cycle, S set to 10 different values ranging from 0.18 % to 1.24 %. At each diameter selected by the DMA (D_b), the number concentration of total aerosol particles (condensation nuclei, CN), N_{CN}, was measured with the CPC, and the number concentration of CCN, N_{CCN}, was measured with the CCNC. The measured CCN activated fractions ($F_{N_{CCN}/N_{CN}}(D_b, S) = N_{CCN}(D_b)/N_{CN}(D_b)$) were corrected for multiply charged particles and fitted with a cumulative Gaussian distribution function as described in Pöhlker et al (2016):

$$F_{\frac{N_{CCN}}{N_{CN}}}(D_b, S) = a\left(1 + erf\left(\frac{D_b - D_{b,a}}{\sigma_a \sqrt{2}}\right)\right), \tag{1}$$

where erf is the error function, a is half the maximum value of $F_{N_{CCN}/N_{CN}}$, $D_{b,a}$ is the dry particle diameter at $F_{N_{CCN}/N_{CN}} = a$, and σ_a is the standard deviation of the cumulative distribution function (CDF). The CCN activation curves were also corrected for differences in counting efficiencies of the CCNC and the CPC (Rose et al., 2010). The following best-fit parameters were determined for each supersaturation: the maximum activated fraction $MAF_F = 2a$, the midpoint activation diameter, $D_{b,a}$, and the CDF standard deviation, σ_a. MAF_F typically equals unity, except for external mixture of CCN-active with CCN-inactive particles, whereby the difference in CCN activity is due to chemical composition and hygroscopicity. While σ_a serves as indicator for the extent of heterogeneity of particle's composition. Calibration aerosols composed of high-purity ammonium sulfate exhibit small non-zero σ_a values that correspond to ~3 % of $D_{b,a}$ and can be attributed to heterogeneities of the water vapor supersaturation profile in the CCNC or other non-idealities such as DMA transfer function and particle shape effects (Rose et al., 2008). Thus, normalized CDF standard deviations or "heterogeneity parameter" values of $\sigma_a/D_{b,a}$ ~ 3 % indicate internally mixed CCN, whereas higher values indicate external mixtures of particles with varying chemical composition and hygroscopicity (Rose et al., 2008; 2010).

2.6 HHTDMA setup and modes of operation

The hygroscopic properties of the subpollen particles were measured in the 2-99.5 % RH range with a high humidity tandem differential mobility analyser (HHTDMA) described elsewhere (Mikhailov and Vlasenko, 2020). Briefly, two separate atomizers (model 3076, TSI, USA) were used for aerosol particles generation: first of them to study aerosol hygroscopic properties, and second for RH determination using ammonium sulfate particles growth factors (Suppl. S3, Fig.S2). The generated aerosol solution droplets were dried to a relative humidity of ~3 % in a Nafion MD-700 dryer (L=60 cm; residence time, RT = 27 s) and then in a silica gel diffusion dryer (SDD, RT= 63 s) to the residual relative humidity of ~2% RH. The dry aerosol was passed through a bipolar charger ([85]Kr) and a

differential mobility analyzer (DMA1) (model 3081, TSI, USA) to select monodisperse particles. This near monodisperse aerosol was then humidified, and the resulting particle size after humidification was measured with the scanning mobility particle sizer (DMA2) (SMPS, model 3080, CPC 3772, AIM version 9.0.0.0, Nov. 11, 2010, all TSI, USA). The particle size distributions measured were fitted with a log-normal distribution function (Origin 9 software), and the median diameter (D_b) of the fit function was used for further data analysis. Throughout the all relative humidity range, the absolute RH uncertainty is less than 0.5 %, and the relative growth factor uncertainty due to RH and instrumental errors does not exceed 1 % (Fig.S3).

Three operation modes are available using this HHTDMA instrument: hydration and dehydration (H&D) also called restructuring mode, hydration, and dehydration. These modes correspond to different sequences of humidification and drying ("RH histories") of aerosol particles, as outlined in Table S2 (Suppl. S3). The H&D mode was used to specify the optimal RH range in which initial irregular particles transform into compact globules. Upon hygroscopic growth study, the H&D mode was *in-situ* coupled with a conventional hydration or dehydration mode. The mobility equivalent particle growth factor, g_b was calculated as the ratio of the mobility equivalent diameter, D_b measured after conditioning (hydration, dehydration) to the minimum mobility diameter $D_{b,H\&D,min}$ observed in the H&D mode:

$$g_b = \frac{D_b}{D_{b,H\&D,min}} \quad . \tag{2}$$

Further details on the HHTDMA operation provided in Suppl.S3.

2.7 Hydrodynamic size distribution of colloidal bioparticles

Aqueous extracts of pollen grains used for aerosol particle generation contain both water-soluble and water-insoluble material. Insoluble material mainly presents in the form of colloidal particles. The presence of colloids in the size-selected particles can affect their hygroscopic properties. To evaluate this effect, we measured the hydrodynamic size distribution of colloidal bioparticles using a dynamic light scattering (DLS) system (model SZ-100, Horiba, Ltd). Measurement parameters were as follows: a laser wavelength of 532 nm (10 mW) a scattering angle of 90º, a measurement temperature of 25 ºC, a medium viscosity of 0.896 mPa·s, a medium refractive index of 1.333, and material refractive index of 1.400. The size distribution of nano-bioparticles was determined in a filtered solution (1 ml) with the same concentration of pollen species as used for dry particle generation (Sect. 2.1). The samples were loaded into quartz microcuvettes, and 7-10 measurements were performed, for which average and standard deviation were calculated. The obtained DLS-based size distributions were converted into number particle size distributions as described in Suppl. S4.

2.8 Aerosol particles shape

Inorganic and organic aerosol particles as well as their mixtures restructure upon humidification below its deliquescence. Irregular envelope shape and porous structure can cause a discrepancy between the mobility equivalent and mass equivalent particle diameters that usually limit precision of mobility diameter-based HTDMA and CCNC experiments (Mikhailov et al., 2004, 2009, 2020; Biskos et al., 2006; Gysel et al. 2004; Rose et al., 2008). To account for restructuring we used the minimum mobility particle diameter, $D_{b,H\&D,min}$ obtained in H&D HHTDMA mode as an approximation of mass equivalent diameter of the dry solute particle, D_s (i.e. $D_s = D_{b,H\&D,min}$.). Based on H&D measurements the dynamic shape factor, χ of the dry initial particles can be estimated as following (DeCarlo et al., 2004):

$$\chi = \frac{D_{b,i} C(D_{b,H\&D,min})}{D_{b,H\&D,min} C(D_{b,i})}, \tag{3}$$

where $D_{b,i}$ is the initial mobility equivalent diameter selected by DMA1 and measured by DMA2, $C(D_{b,H\&D,min})$ and $C(D_{b,i})$ are the Cunningham slip correction factors for the respective diameters $D_{b,H\&D,min}$ and $D_{b,i}$. χ can be split into a component β which describes the shape of the particle envelope and a component δ which is related to the particle porosity and allows the calculation of the void fraction inside the particle envelope f (Brockmann and Rader, 1990):

$$\chi = \beta\delta \frac{C(D_{h\&d,min})}{C(D_{h\&d,min}\delta)} \tag{4}$$

$$f = (1 - \delta^{-3}) \tag{5}$$

2.9 κ-Köhler model and effective hygroscopicity parameters

Both HTDMA and CCN data were fitted by the Köhler model introduced by P&K (Petters and Kreidenweis, 2007) to obtain an effective hygroscopicity parameter, κ, which is a measure of the amount of water bound per unit volume of dry solute. The saturation ratio, s, over an aqueous solution droplet is expressed in both sub- and supersaturated regimes by the κ-Köhler model:

$$s = a_w \times Ke = \frac{D_{wet}^3 - D_s^3}{D_{wet}^3 - D_s^3(1-\kappa)} \times exp\left(\frac{4\sigma_w M_w}{\rho_w R T D_{wet}}\right), \tag{6}$$

where a_w is the water activity, Ke is the Kelvin term, D_s is the mass equivalent diameter of the dry solute particle, D_{wet} is the diameter of the solution droplet, σ_w is the solution surface tension for pure water (72 mNm^{-1}), which is used here to produce a self-consistent data set as suggested in $P\&K$, M_w is the molecular weight of water, ρ_w is the density of water, R is the universal gas constant, T is the

temperature. The hygroscopicity, $\kappa_{b,a}$ from CCN data set was obtained by inserting the CCN-derived dry activation diameter $D_{b,a}$ for D_s and varying both κ and D_{wet} until the saturation ratio $s = $ RH/100 % was equivalent at the same time to the prescribed supersaturation $S = (s\text{-}1)100$ % and to the maximum of a Köhler model curve of CCN activation. The same procedure was used to calculate the corrected hygroscopicity κ_a due to irregularity shaped structure of the initial dry particles (Sect. 3.3; Eq.11). In this case, the restructured diameter, D_a was inserted for D_s. Combining water activity, a_w from Eq. (6) and Eq.(2) gives:

$$\kappa_b = \frac{(g_b^3 - 1)(1 - a_w)}{a_w}, \tag{7}$$

where κ_b refers to the HHTDMA-measured hygroscopicity κ. The uncertainty for κ_a and κ_b was calculated as propagated error (Suppl. S5). To convert the measured RH-based growth curves (g_b vs. RH) into activity-based curves (g_b vs. a_w) we divided the RH values through the Kelvin term of Eq.(6) assuming that σ is equal to surface tension of pure water (72 mN m^{-1}).

As proposed by Kreidenweis et al. (2005), hygroscopic growth curves can be approximately described with a polynomial three-parameter fit function of the following form:

$$g_b = \left(1 + [k_1 + k_2 a_w + k_3 a_w^2]\frac{a_w}{1 - a_w}\right)^{1/3}, \tag{8}$$

where adjustable parameters k_1, k_2, and k_3 capture non-ideality, caused by mixing between water and solutes. From Eqs. (7) and (8) the dependence of κ_b on a_w can be described by:

$$\kappa_b = k_1 + k_2 a_w + k_3 a_w^2 \tag{9}$$

3 Experimental results and discussion

3.1 Chemical composition of pollen species

Bulk chemical analysis results of water-extractable compounds are summarized in Table 1 and illustrated in Fig. 1. Their mass fraction, w_i was determined as described in Sect. 2.2. According to the chemical and gravimetrical analysis, the fraction of the total dissolved species varies from ~35 wt % (pine and rapeseed samples) to ~ 61 wt % (birch sample). Among them the major components are carbohydrates (i.e. ~28 wt % for birch and rapeseed and 51 wt % for pine pollen solution) followed by inorganic ions (<10 wt %). The most common soluble carbohydrates in pollen grains are monosaccharides (glucose, fructose) and disaccaharydes (sucrose, maltose). Other soluble carbohydrates such as raffinose, stachyose, rhamnose, and arabinose can persist in a lesser amount (Stanley and Linskens, 1974). Water-extractable starch in the filtered solution is 2, 1, and 0.8 wt % for birch, pine and rapeseed solution, respectively (Table 1). However, extractable starch contain only

minor part of resistant starch measured in pollen grains as described in Sect. 2.4.3. The mass ratio of water-extractable to resistant starch is ~ 9 % (birch), ~ 3% (pine), and ~ 7% (rapeseed) by weight (not shown in Table 1). Protein is the second most abundant organic component after carbohydrates. Its content in the filtered extracts varies from ~ 0.3 wt % (pine pollen) to ~ 3 wt % (birch pollen). DNA in negligible quantities was detected in birch and pine aqueous extracts. Phosphorus in the form of PO_4^{3-} and K^+ are the dominant inorganic ions and account for ~ 3 wt % of the extractable material. All filtered pollen extracts contain a small amount of SO_4^{2-} ion varying from 0.3 wt % (birch pollen extract) to 2 wt % (pine pollen extract). Calcium and magnesium are also present in the filtered
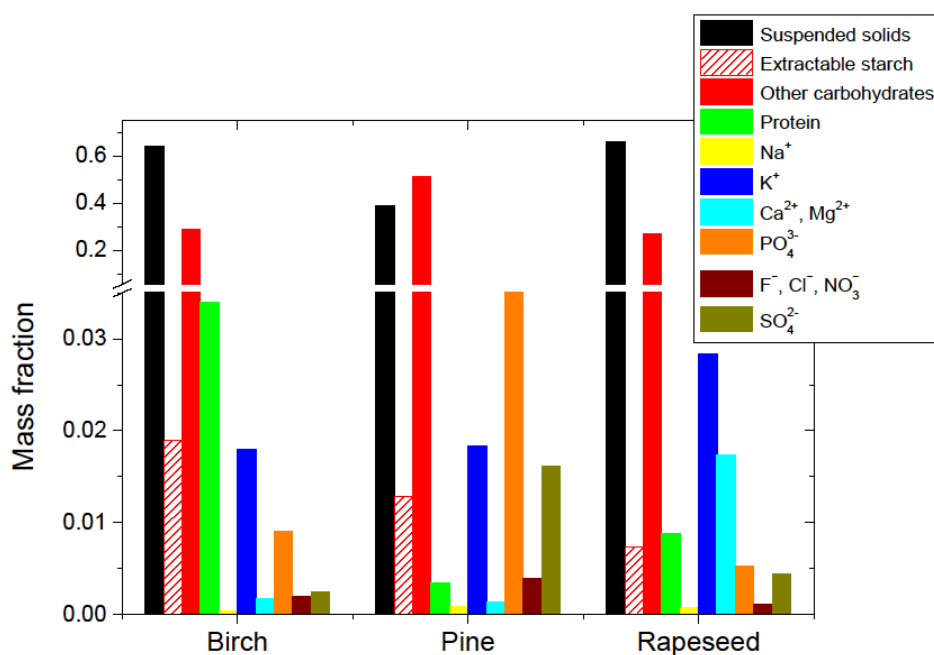
Fig. 1. Mass fraction of dissolved and suspended species in the filtered solution of pollen grains.

pollen solutions. Their highest total value of ~ 1 wt % was found in the rapeseed sample (Table 1). Other ions such as Na^+, F^-, Cl^- and NO_3^- were found in small amounts. Their total mass ratio does not exceed 0.3 wt %. The biological role of the above chemical species during pollen grains development and maturation is considered elsewhere (Baker and Baker, 1979; Pacini, et al., 1999; Roulston et al., 2000; Stanley and Linskens, 1974). Based on the chemical analysis results, it is reasonable to assume that water-soluble sugars, proteins, and inorganic ions are the main components that causing water uptake by pollen subparticles. Table 1 shows that the mass ratio of water-insoluble compounds in the filtered solutions is significant with amounts up 39, 64 and 66 wt % of pine, birch and rapeseed extracts, respectively. These suspended particles (hydrosols or colloids) can comprise cross-linked sporopollenin, callose, carotenoids, cellulose, starch, and sterols in various proportions (Pacini and Hesse, 2005; Stanley and Linskens, 1974). We consider this fraction of pollen species as an inert

Table 1. Concentration (µg ml^{-1}) and mass fraction (w_i) of chemical species (i) in the filtered solution of pollen grains. Total solids is the sum of the total dissolved species and total suspended solids. w_i is the ratio of the amount of selected species to the mass of total solids containing in 1 mL of water.

Chemical species	Birch		Pine		Rapeseed	
	µg ml^{-1}	w_i	µg ml^{-1}	w_i	µg ml^{-1}	w_i
Carbohydrates	190 ± 8	0.29	299 ± 11	0.51	252 ±15	0.27
Water- extractable starch	12.4 ± 8.0	0.02	7.4 ± 5.9	0.01	6.8 ± 7.2	0.008
Protein	22.0 ± 3.8	0.03	2.00 ± 0.15	0.003	8.22 ± 0.19	0.009
DNA	0.018 ± 0.002	2.7×10^{-5}	1.6×10^{-4}	$< 3 \times 10^{-7}$	-	-
Na^+	0.28 ± 0.02	4.2×10^{-4}	0.52 ± 0.01	9.0×10^{-4}	0.62 ± 0.02	6.7×10^{-4}
K^+	11.77 ± 0.03	0.02	10.69 ± 0.03	0.02	26.44 ± 0.64	0.03
Ca^{2+}	0.65 ± 0.01	0.001	0.35 ± 0.01	6.0×10^{-4}	11.30 ± 0.23	0.01
Mg^{2+}	0.46 ± 0.01	0.001	0.41 ± 0.01	7.1×10^{-4}	4.90 ± 0.04	5.2×10^{-3}
F^-	0.46 ± 0.02	0.001	0.18 ± 0.01	3.1×10^{-4}	0.12±0.03	1.3×10^{-4}
Cl^-	0.78 ± 0.06	0.001	1.19 ± 0.08	2.1×10^{-3}	0.89±0.03	9.6×10^{-4}
NO_3^-	-	-	0.90 ± 0.02	1.5×10^{-3}	-	-
PO_4^{3-}	5.97 ± 0.17	0.009	29.7 ± 0.9	0.05	4.96 ± 0.08	0.005
SO_4^{2-}	1.64 ± 0.01	0.003	9.42 ± 0.14	0.02	4.06 ± 0.08	0.004
All ions	22.0 ± 0.3	0.03 ± 0.01	53.3 ± 1.2	0.09 ± 0.01	53.4 ± 1.1	0.06 ± 0.01
All dissolved organics	212 ± 21	0.33 ± 0.03	301 ± 17	0.52 ± 0.03	261 ± 16	0.28 ± 0.02
Total dissolved species	234 ± 13	0.36 ± 0.04	354 ± 12	0.61 ± 0.03	313 ± 17	0.34 ± 0.02
Total suspended solids	418 ± 17	0.64 ± 0.03	227 ± 20	0.39 ± 0.04	616 ±19	0.66 ± 0.03
Total solids	652 ± 4	1.00 ±0.05	581 ± 16	1.00 ± 0.08	930 ± 9	1.00 ± 0.02

material that suppresses hygroscopic growth and CCN activity of subpollen particles, as discussed below.

3.2 Hydrodynamic size distribution of hydrosols

As shown in Sect. 3.1 the mass fraction of suspended particles in the nebulized solution is significant (39-66 wt %). Together with concentration, the effect of such hydrosols on the hygroscopicity of the DMA-selected particles is highly dependent on their size range. Figure 2 shows the hydrodynamic size distribution of colloidal bioparticles determined by a DLS system using the conversion algorithm described in Suppl. S4. The obtained results clearly show that the size of colloidal particles spans the range of 40-110 nm, which is within the SPP size range of dry particles (20-190 nm) used for CCN and HHTDMA measurements. It follows that the studied subpollen particles are an internal mixture of water-soluble and water-insoluble (suspended) compounds in different proportions. Besides,

colloidal particles tend to coagulate, forming aggregates. This aging process can lead to a different composition of the size-selected dry particles during the HHTDMA or CCN experiments.
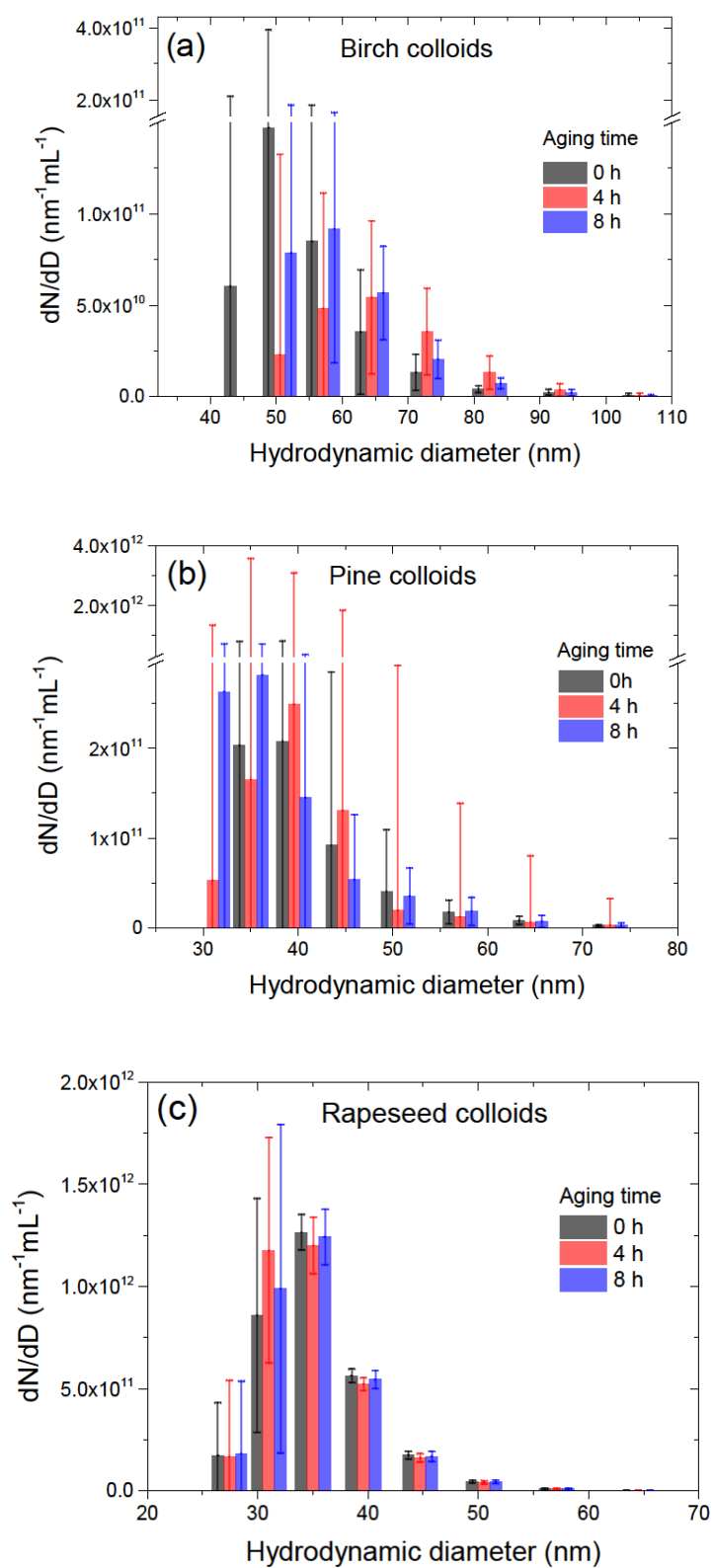
Fig. 2. Colloidal particles number size distribution of aqueous extracts of birch (**a**), pine (**b**) and rapeseed (**d**) pollen grains**:** initial, (0 h) and after 4h and 8 h aging, respectively.

A simple time-dependent turbidity test with an aqueous birch pollen extract demonstrates that this effect becomes noticeable only after 10 h of aging (Suppl. S6, Fig. S.5). Experiment with dynamic light scattering provides a similar result. Figure 2 shows that for a typical time scale of CCN (~ 4 h) and HHTDMA (~ 8 h) measurements, the size distributions of birch, pine and rapeseed colloids remain constant within the uncertainty range, indicating that coagulation of suspended particle is small and therefore does not lead to a noticeable change in the size-selected dry particles composition in the specified time periods.

3.3 Particles restructuring

The H&D HHTDMA operation mode was first used to study the size-dependent aerosol particle restructuring ($D_{b,i}$ = 30–180 nm). The dried aerosol particles selected by DMA1 entered to the pre-conditioning section (Fig.S2, dashed rectangle), underwent microstructural transformation, acquiring a more compact/spherical microstructure, during a cycle of humidification (H1, RT = 0.5 s) and drying (Nafion MD-700, RT = 27 s; SDD, RT = 16 s) (Mikhailov et al., 2004; 2009). The particles growth factor obtained during the H&D experiment was calculated as follows: $g_{H\&D} = D_{b,RH}/D_{b,i}$, where $D_{b,RH}$ is the mobility particle diameter measured at RH = RH2 (Table.S2).

Figure 3 illustrates the measurement of the subpollen particles growth factors in H&D mode. All species exhibit restructuring, i.e. the growth factors decrease with increasing RH, wherein this effect is strongest for largest diameters. It is also seen that for birch and pine SPP the $g_{H\&D,min}$ is already reached at ~ 35 % RH, while for rapeseed SPP the $g_{H\&D,min}$ values are observed at higher humidity starting from ~ 65 % RH (excluding particles with $D_{b,i} < 60$ nm). The size-dependent $RH_{H\&D,min}$ intervals used to $g_{H\&D,min}$ averaging are shown in Table 2. The $RH_{H\&D,min}$ range for ~100 nm particles was further employed in HHTDMA hydration/dehydration experiments to convert *in-situ* irregular initial particles into compact globules. Figure 4 shows the growth factors, $g_{H\&D,min}$ obtained over the $D_{b,i}$ range of 30–180 nm together with an exponential fitting curve,

$$g_{b,H\&D,min} = \eta + \varphi exp\left(-\frac{D_{b,i}}{\tau}\right), \tag{10}$$

where η, φ, and τ are the best fit parameters listed in Table S3. The fit values of $g_{H\&D,min}$ are further used for particles shape correction of initial dry activation diameters, $D_{b,a}$ determined in size-resolved CCN experiments:

$$D_a = g_{b,H\&D,min}D_{b,a} . \tag{11}$$
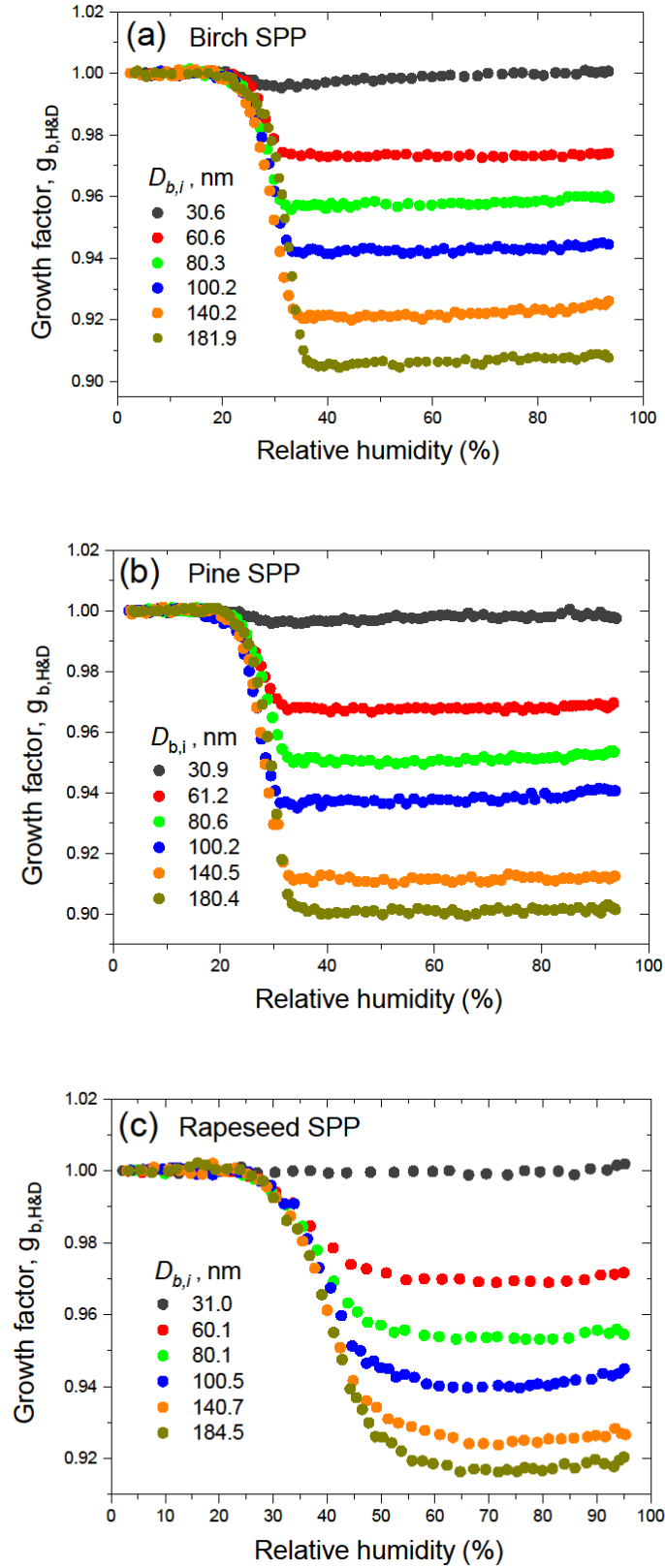
Fig. 3. Growth factors ($g_{b,H\&D}$) of birch **(a)**, pine **(b)** and rapeseed **(c)** SPP as a function of relative humidity observed for different initial mobility diameters ($D_{b,i}$) in hydration&dehydration (H&D) HHTDMA experiments.

Table 2. The size-dependent microstructural rearrangement parameters of subpollen particles (SPP) obtained in H&D experiment. $D_{b,i}$ and $g_{b,H\&D,min}$ are mean ($\pm$ 2 SD) initial mobility diameter and minimum mobility growth factor, respectively. The dynamic shape factor (χ), porosity (δ), and void fraction (f) together with propagated error (Δf) are calculated from Eq.(3), Eq.(4), and Eq.(5), respectively. For birch, pine, and ~30 nm rapeseed SPP the shape particle envelope (β) is set to 1; for rapeseed SPP at $D_{b,i} > 30$ nm the β values were obtained as described in Suppl. S8. $RH_{b,H\&D,min}$ is the relative humidity at which the minimum mobility growth factors were observed.

$D_{b,i}$ (nm)	$g_{b,H\&D,min}$	χ	β	δ	$f \pm \Delta f$ (%)	$RH_{H\&D,min}$ (%)
Birch SPP						
30.56 ± 0.04	0.997± 0.002	1.006	1	1.003	0.9 ± 1.0	28 – 36
60.59 ± 0.05	0.973 ± 0.001	1.051	1	1.028	7.9 ± 0.4	33 – 50
80.32 ± 0.12	0.957 ± 0.002	1.082	1	1.045	12.4 ± 0.7	33 – 50
100.21 ± 0.08	0.942 ± 0.001	1.110	1	1.061	16.3 ± 0.5	33 – 50
140.18 ± 0.20	0.921 ± 0.002	1.146	1	1.085	21.7 ± 0.5	34 – 50
181.86 ± 0.08	0.906 ± 0.001	1.169	1	1.104	25.7 ± 0.5	38 – 54
Pine SPP						
30.95 ± 0.02	0.996 ± 0.001	1.007	1	1.004	1.1 ± 0.4	29 – 40
61.19 ± 0.07	0.968 ± 0.003	1.062	1	1.033	9.3 ± 1.2	33 – 50
80.58 ± 0.06	0.950 ± 0.002	1.096	1	1.052	14.1 ± 0.6	35 – 58
100.20 ± 0.15	0.937 ± 0.002	1.121	1	1.067	17.7 ± 0.8	33 – 58
140.45± 0.17	0.911 ± 0.002	1.166	1	1.097	24.3 ± 0.7	33 – 60
180.41± 0.20	0.901 ± 0.002	1.179	1	1.110	26.9 ± 0.5	39 – 62
Rapeseed SPP						
31.03 ± 0.04	0.999 ± 0.002	1.002	1	1.001 ± 0.003	<1	65 – 85
60.06 ± 0.04	0.969 ± 0.001	1.060	1.03 ± 0.02	1.02 ± 0.02	4.9 ± 6.2	75 – 85
80.12 ± 0.02	0.953 ± 0.001	1.090	1.03 ± 0.02	1.03 ± 0.02	8.8 ± 4.3	61 – 82
100.50 ± 0.02	0.940 ± 0.001	1.114	1.04 ± 0.03	1.04 ± 0.02	11.1 ± 5.3	70 – 82
140.71± 0.15	0.925 ± 0.002	1.138	1.07 ± 0.03	1.04 ± 0.02	11.4 ± 6.2	66 – 80
184.47± 0.12	0.917 ± 0.002	1.146	1.09 ± 0.02	1.03 ± 0.02	9.3 ± 5.2	66 – 82
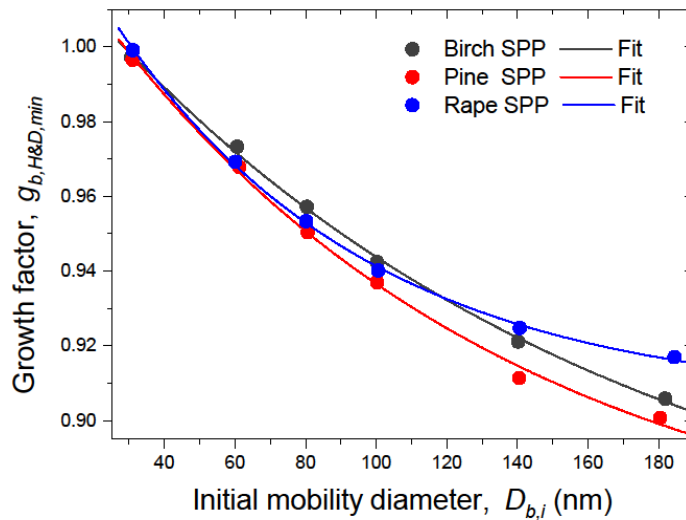
Fig. 4. Minimum mobility growth factors ($g_{b,H\&dD,min}$) of birch, pine, and rapeseed subpollen particles as a function of initial mobility diameter ($D_{b,i}$). Line is the exponential fit function with the best fitting parameters listed in Table S3.

3.4 Dry particles morphology

Using Eq. (3) and assuming that $D_{b.H\&D,min}$ obtained in H&D mode is equal to D_s we calculated the size-dependent dynamic shape factor of the SPP, χ (Table 2). Scanning electronic microscope (SEM) images of the initial birch and pine SPP show a spherical shape (Fig.5a and 5b), therefore, one can accept that $\beta = 1$. Using Eq. (4) and Eq. (5) we estimated the porosity (δ) and void fraction (f) of birch and pine SPP depending on their size (Table 2).
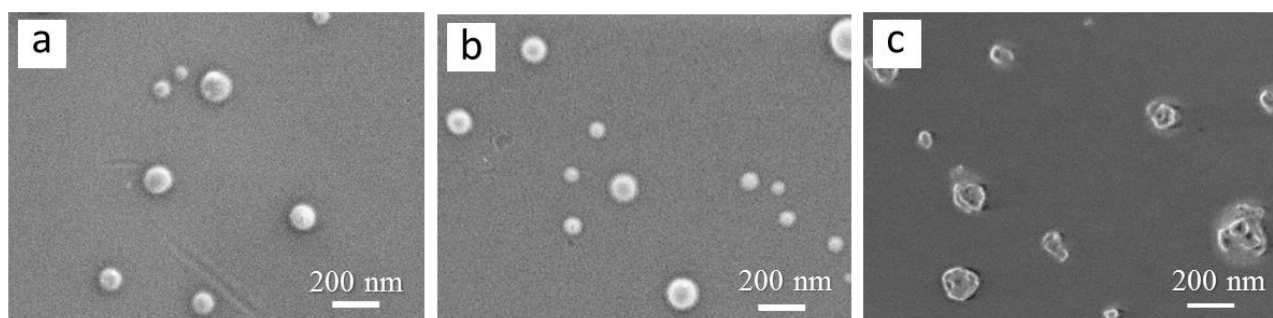
Fig. 5. SEM images of birch (a), pine (b), and rape (c) subpollen particles.

The obtained results indicate that despite the spherical shape the initial dry particles have a porous structure, wherein the void fraction gradually increases with their size, reaching ~26 % for particles of ~180 nm. Figure 5c shows that in contrast to birch and pine SPP the rapeseed particles external morphology is not spherical. To estimate the envelope component β of rapeseed SPP we used Eq. (S8), approximating their shape by prolate ellipsoid as described in Suppl. S8. The resulting microstructural parameters of rapeseed SPP are listed in Table 2. Note that δ and f values obtained in this way are their upper estimate, since it is assumed that all particles are oriented in both DMA to its flow by maximal axis. In addition, due to technical limitation of SEM for 30 nm particles the β was set to 1. Even with these assumptions, the void fraction in rapeseed particles is on average 2-fold less than that for birch and pine particles (Table 2). According to chemical analyses (Table 1), rapeseed extracts contain the highest amount of calcium (~11 µg ml⁻¹) and undissolved species (~620 µg ml⁻¹). Since calcium is mainly present in the walls of the pollen grains, it is reasonable to assume that the irregular morphology of rapeseed SPP (Fig. 5c) is due to the predominant aggregation of exine and intine species such as cross-linked sporopollenin and cellulose (Stanley and Linskens, 1974).

3.5 CCN properties

The average parameters derived from CCN activation curves as a result of three repeated measurements for each sample are summarized in Table 3. Figure 6 shows the maximum activation fraction (MAF_F) (panel **a**) and normalized standard deviations ($\sigma_a/D_{b,a}$) (panel **b**) against the

corresponding midpoint activation diameters ($D_{b.a}$) and supersaturation (S %) obtained in a series of three CCN measurements for each type of SPP.
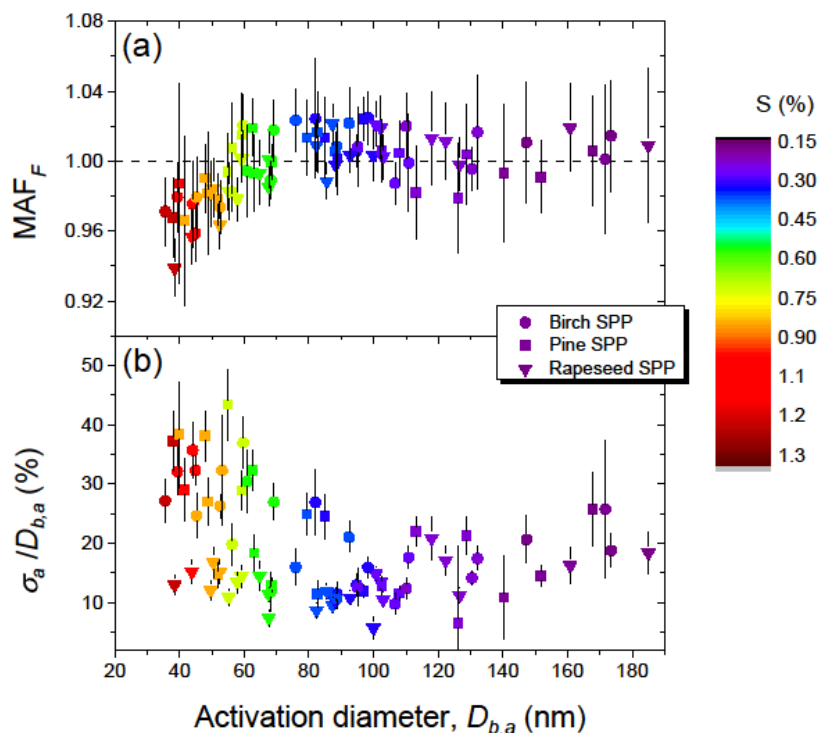
Fig. 6. Characteristic parameters of birch, pine and rapeseed subpollen particles derived from CCN activation curves: maximum activated fraction (MAF_F) (**a**) and heterogeneity parameter ($\sigma_a/D_{b,a}$) (**b**).

For particles with $D_{b,a} > 80$ nm the MAF_F is close to one (Fig.6a) and $\sigma_a/D_{b,a}$ (Fig. 6b) ranges from 10 % to 25 %, which implies that nearly all aerosol particles larger ~80 nm were CCN-active at S smaller 0.5 %. As detailed in Sect. 2.5, $\sigma_a/D_{b,a}$ characterizes the heterogeneity of CCN-active particles in the size range around $D_{b,a}$. The observed 10-25 % heterogeneity range is clearly higher than the ~3% observed for aerosols of homogeneous chemical composition, indicating that the particles in this size range were not internally mixed with respect to their solute content (Rose et al., 2010; Pöhlker et al. 2018). For particles with $D_{b,a}$ smaller ~ 70 nm (S > 0.6 %) the MAF_F is below one (Fig.6a) dropping to ~ 0.93 and $\sigma_a/D_{b,a}$ is high reaching up to 30-40 % for birch and pine subpollen particles (Fig. 6b). Both results indicate the presence of a noticeable fraction of CCN-inactive particles with much lower hygroscopicity. As shown in Sect. 3.2 the nebulized aqueous extracts contain a substantial proportion of colloidal particles in the size range of 20-80 nm (Fig. 2). It is therefore possible, that a certain fraction of these particles did not have a sufficient amount of dissolved compounds on the surface, which prevented their activation even at S > 1% (Fig.6a).

Due to porosity and non-sphericity of the initial dry particles, the shape corrected activation diameters (Eq.11), D_a are lower than those initial CCN measured diameters, $D_{b,a}$ (Table 3).

Table 3. Characteristic average CCN parameters (mean values ± SD) for subpollen particles (SPP) at different S (%) obtained in a series of three measurements for each sample. Quantities are a maximum activated fraction, MAF_F, heterogeneity parameter, $\sigma_a/D_{b,a}$, initial, $D_{b,a}$, $\kappa_{b,a}$ and shape corrected, D_a, κ_a dry diameter and hygroscopicity parameter, respectively. $\delta\kappa$ is the relative change in hygroscopicity due to particles restructuring, and $D_{wet,a}$ is the wet activation diameter.

S	MAF_F	$\sigma_a/D_{b,a}$	$D_{b,a}$	D_a	$D_{wet,a}$	$\kappa_{b.a}$	κ_a	δk
(%)		(%)	(nm)	(nm)	(nm)			(%)
Birch SPP								
0.18 ± 0.01	1.01 ± 0.04	21.8 ± 6.1	150 ± 4	137 ± 3	783 ± 44	0.11 ± 0.02	0.13 ± 0.02	18 ± 4
0.23 ± 0.02	1.01 ± 0.02	14.7 ± 1.6	125 ± 2	117 ± 2	659 ± 31	0.12 ± 0.02	0.15 ± 0.02	21 ± 4
0.28 ± 0.02	1.00 ± 0.02	13.4 ± 2.3	106 ± 2	100 ± 2	508 ± 18	0.15 ± 0.02	0.18± 0.03	17 ± 3
0.32 ± 0.02	1.02 ± 0.02	18.7 ± 3.0	95 ± 2	90 ± 2	433 ± 13	0.15 ± 0.03	0.18 ± 0.03	16 ± 3
0.37 ± 0.03	1.02 ± 0.02	16.0 ± 2.2	91 ± 2	86 ± 2	378 ± 10	0.13 ± 0.02	0.16 ± 0.02	13 ± 3
0.57 ± 0.05	1.00 ± 0.02	23.1 ± 3.9	79 ± 2	75 ± 1	251 ± 4	0.13 ± 0.02	0.15 ± 0.03	11 ± 2
0.71 ± 0.05	0.99 ± 0.02	27.2 ± 3.3	70 ± 1	67 ± 1	201 ± 3	0.14 ± 0.02	0.16 ± 0.02	10 ± 2
0.85 ± 0.06	0.98 ± 0.04	30.3 ± 5.1	60 ± 3	52 ± 3	168 ± 2	0.13 ± 0.03	0.14 ± 0.03	10 ± 2
1.04 ± 0.07	0.97 ± 0.02	31.8 ± 3.6	45 ± 1	44 ± 1	137 ± 2	0.14 ± 0.02	0.15 ± 0.03	11 ± 4
All						0.13 ± 0.02	0.16 ± 0.03	
Pine SPP								
0.18 ± 0.01	1.00 ± 0.03	17.0 ± 3.3	148 ± 16	134 ± 14	774 ± 43	0.13 ± 0.04	0.17 ± 0.05	23 ± 8
0.23 ± 0.02	0.99 ± 0.03	16.6 ± 2.2	124 ± 8	115 ± 7	616 ± 27	0.14 ± 0.03	0.17 ± 0.03	20 ± 4
0.28 ± 0.02	1.01 ± 0.02	12.3 ± 1.3	104 ± 4	97 ± 3	507 ± 18	0.16 ± 0.02	0.19 ± 0.02	18 ± 2
0.33 ± 0.02	1.01 ± 0.02	15.9 ± 2.3	91 ± 5	86 ± 5	434 ± 13	0.17 ± 0.03	0.20 ± 0.03	15 ± 3
0.37 ± 0.03	1.01 ± 0.02	15.9 ± 2.2	85 ± 5	81 ± 5	378 ± 10	0.16 ± 0.03	0.18 ± 0.03	14 ± 3
0.56 ± 0.04	1.00 ± 0.02	21.2 ± 2.5	73 ± 17	70 ± 15	252 ± 4	0.16 ± 0.02	0.17 ± 0.03	10 ± 6
0.71 ± 0.05	1.01 ± 0.02	30.7 ± 3.5	66 ± 18	64 ± 16	201 ± 3	0.15 ± 0.02	0.16 ± 0.02	8 ± 5
0.85 ± 0.06	0.98 ± 0.02	26.6 ± 3.1	56 ± 12	54 ± 11	167 ± 2	0.15 ± 0.02	0.16 ± 0.02	6 ± 4
1.04 ± 0.07	0.97 ± 0.05	29.0 ± 5.3	42 ± 2	41 ± 1	137 ± 2	0.17 ± 0.02	0.18 ± 0.02	6 ± 2
1.24 ± 0.09	0.98 ± 0.04	37.8 ± 7.0	39 ± 1.4	38 ± 1	116 ± 2	0.15 ± 0.02	0.16 ± 0.02	10 ± 4
All						0.15 ± 0.04	0.18 ± 0.04	
Rapeseed SPP								
0.18 ± 0.01	1.01 ± 0.03	17.3 ± 3.3	174 ± 19	159 ± 15	784 ± 43	0.11 ± 0.03	0.12 ± 0.03	8 ± 3
0.23 ± 0.02	1.01 ± 0.02	16.4 ± 2.4	122 ± 4	114 ± 4	614 ± 26	0.16 ± 0.02	0.18 ± 0.02	11 ± 1
0.28 ± 0.02	1.01 ± 0.01	13.0 ± 1.2	102 ± 1	96 ± 1	510 ± 18	0.18 ± 0.02	0.20 ± 0.02	9± 1
0.32 ± 0.02	1.00 ±0.01	9.0 ± 1.4	94 ± 6	89 ± 5	435 ± 13	0.18 ± 0.03	0.19 ± 0.03	4 ± 1
0.37 ± 0.03	1.01 ±0.01	10.1 ± 1.2	85 ± 3	81 ± 2	379 ± 10	0.17 ± 0.01	0.19 ± 0.02	9 ± 1
0.57 ± 0.04	0.99 ±0.02	11.1 ± 1.7	67 ± 2	64 ± 2	251 ± 4	0.15 ± 0.01	0.16 ± 0.01	6 ± 1
0.71 ± 0.05	0.99 ± 0.02	12.9 ± 1.7	57 ± 2.0	56 ± 2	200 ± 3	0.16 ± 0.02	0.16 ± 0.02	1 ± 1
0.85 ± 0.06	0.98 ± 0.02	14.7 ± 2.1	51 ± 2	50 ± 2	167 ± 2	0.15 ± 0.06	0.15 ± 0.01	4 ± 1
1.04 ± 0.07	0.96 ± 0.02	15.3 ± 2.0	44 ± 2	43 ± 1	138 ± 2	0.15± 0.02	0.16± 0.02	5 ± 2
1.24 ± 0.09	0.94 ± 0.02	13.0 ± 1.7	39 ± 1	38 ± 1	116 ± 2	0.15 ± 0.02	0.16 ± 0.02	3 ± 1
All						0.16 ± 0.02	0.17 ± 0.02	

This difference leads to a significant underestimation of the κ values, especially for large particles (Table 3). Figure 7 illustrates the monotonous growth of $\delta\kappa = (\kappa_a - \kappa_{b,a})/\kappa_a$ with D_a increasing,
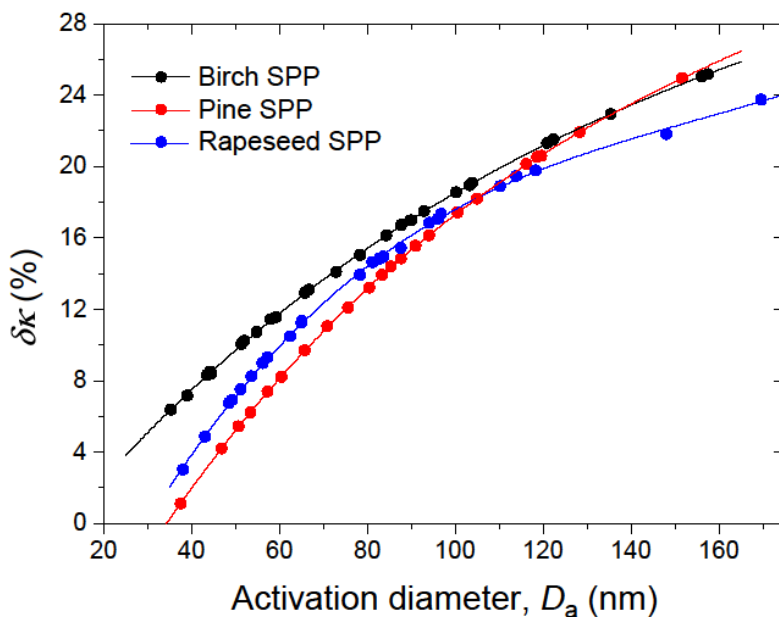
Fig. 7. The relative change of the hygroscopicity parameter uncertainty, $\delta\kappa$ due to particle irregular structure as a function of activation diameters, D_a. Lines are 3-power polynomial fit to guide the eye.

reaching ~25 % at D_a ~ 160 nm for birch and pine SPP.

The shape corrected hygroscopicity, κ_a values are shown in Fig. 8. For pine, rapeseed and birch SPP, average κ_a (± SD) is 0.18 ± 0.03, 0.17 ± 0.030 and 0.16 ± 0.02, respectively (Table 3), indicating that the difference in mean κ_a values is not statistically significant. However, noticeable size-dependent variations in SPP hygroscopicity are traced. Aerosol particles in the size range of 80-120 nm are more hygroscopic (κ_a ~ 0.20) than these in the range from 35 to 70 nm (κ_a ~ 0.14) and above 130 nm (κ_a ~ 0.13). The observed variations in κ_a are due to the size-dependent ratio of water-soluble and water-insoluble material in the generated dry particles. As discussed above, enternally mixed particles with D_a < 70 nm are enriched in primary non-hygroscopic colloids (Fig.2), while particles with D_a > 130 nm may contain their aggregates.

In general, the CCN measurement results show that the subparticles of pollen grains at sizes exceeding 45 nm are CCN-active at supersaturations below 1 % (Fig.6a) and, therefore, can participate in the formation and modification of cloud systems.
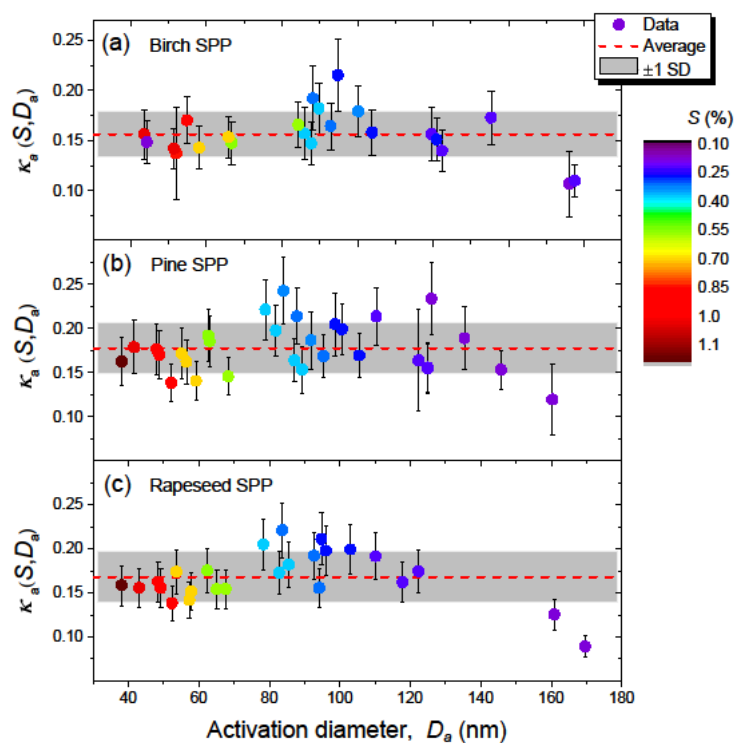
Fig. 8. Shape corrected hygroscopicity, κ_a as a function of aerosol particles activation diameter, D_a and supersaturation, S (color code) of birch (a), pine (b) and rapeseed (c) subpollen particles. The red line and gray shaded area correspond to average $\kappa_a \pm$ SD.

3.6 Hygroscopic properties

To avoid the uncertainties associated with the aerosol particles morphology, we coupled H&D mode with one of the hygroscopic growth mode, as shown in Fig.S2 and previously described in Mikhailov et al. (2020). During the hygroscopic growth experiment, the RH2 values in the pre-conditioning section were maintained in the $RH_{H\&D,min}$ range (Table 2). This range corresponds to $D_{b.H\&D,min}$ values which are used to approximate the actual mass equivalent diameter of dry particles. Using Eq. (2) the measured RH-dependent mobility particle diameters D_b were converted into hygroscopic growth factors. The experimental growth factors obtained upon hydration and dehydration of preconditioned SPP are illustrated in Fig.9 (panels **a**, **c**, **e**). All samples exhibit gradual and fully reversible water uptake similar to the behavior of amorphous organic substances (Mikhailov et al., 2009; 2013). The fact that the hydration and dehydration curves practically coincide also indicates that there are no kinetic limitations in the water uptake/release on the time scale of the HHTDMA experiment (~7 s). Even at low RH, the growth factor of ~100 nm particles preconditioned at RH ~96 % (dehydration mode) is equal to that obtained in the hydration mode. The observed gradual water uptake/release is determined by the specific chemical composition of SPP comprising a broad spectrum of hydrophilic and hydrophobic organic species as well as inorganic ions (Table 1). Such systems tend to adopt amorphous phase states (Mikhailov et al., 2009; Koop et al., 2011; Shiraiwa et al., 2011).
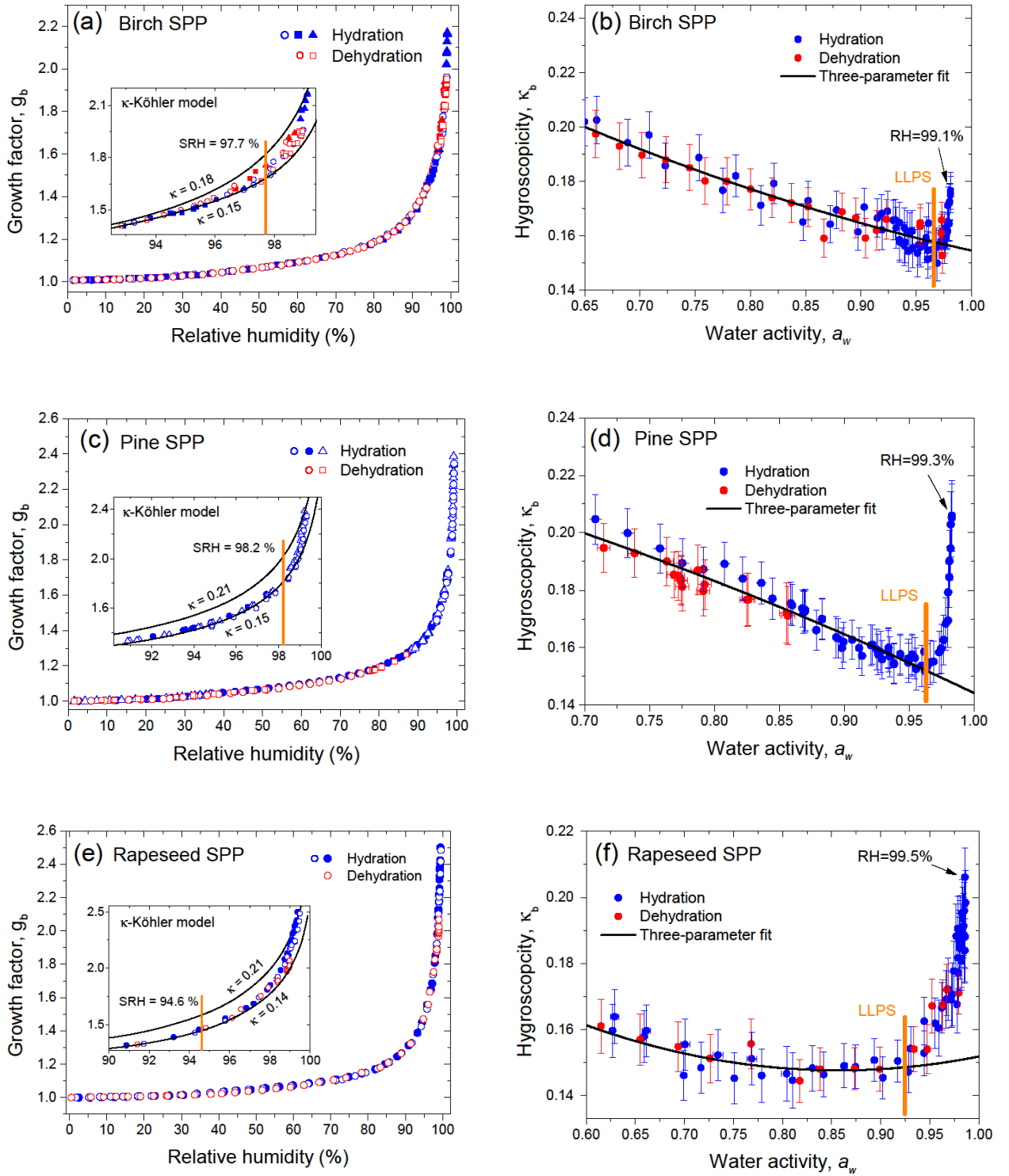
Fig. 9. Growth factors observed in hydration and dehydration experiments (panels **a, c, e**) and g_b-based hygroscopicity parameter, κ_b (Eq.7) (panels **b, d, f**) of birch, pine and rapeseed subpollen aerosol particles with $D_{b,H\&D,min}$ ~ 95 nm, respectively. Different symbols are different experimental runs. Inserts in panels (**a**), (**c**) and (**e**) show the κ-Köhler curves with lowest and highest κ taken from the right panels. The orange vertical line in panels (**b**), (**d**), (**f**) marks the expected onset of LLPS and the arrow shows the experimental point with the maximum RH value obtained in each measurement.

Panels (**a**), (**c**), (**e**) of Fig.9 show that noticeable water uptake by SPP begins at ~30 % RH. Most likely, above this RH value, the particles undergo a moisture-induced phase transition from glass to semi-solid state that can absorb water and swell (Mikhailov et al., 2009; Koop et al., 2011). Continued absorption observed at RH > 30 % converts the semi-solids particles into heterogeneous solution droplets. At RH > 95 %, the particles take up a significant amount of water, with further RH increasing, particle uptake more, and more water leading to an abrupt increase in the growth factors. Thus, in case of pine SPP (Fig.9c), a ~1% change in RH from 98 % to 99.2 % results in a 3-fold increase in the particle volume.

Panels (**b**), (**d**), (**f**) of Fig. 9 show the HHTDMA-derived hygroscopicity parameter, κ_b as a function of water activity for birch, pine, and rapeseed SPP, respectively calculated from Eq. (7). At the a_w range from ~0.6 to ~0.95 a pronounced decreasing trend of κ_b is observed for all samples. Further growth in water activity ($a_w > 0.95$) leads to a sharp increase in the hygroscopicity parameter. The obtained $g_b(RH)$ and $\kappa_b(a_w)$ dependencies are typical for non-ideal multicomponent systems undergoing liquid-liquid phase separation (LLPS) at high RH.

Modeling results by Renbaum-Wolf (2016) and Rastak et al. (2017) using AIOMFAC (Aerosol Inorganic–Organic Mixtures Functional groups Activity Coefficients), as well as these by Liu et al. (2018) based on the Flory-Huggins model show the similar humidity-dependent hygroscopicity for the multicomponent organic material. At $a_w < 0.95$, the thermodynamic models predict high κ values due to strong interaction among different kinds of molecules that gradually decrease with particle dilution and a sharp increase of κ at $a_w > 0.95$ caused by spinodal decomposition resulting in two phases. Above this a_w, the formation of an additional phase becomes thermodynamically favorable in comparison to a single phase. We suggest that consideration of liquid-liquid phase separation, leading to the formation of organic-rich and water-rich phases, can explain the evolution of hygroscopic properties of SPP. Before the liquid-liquid phase separation relative humidity (SRH), the water uptake represents hygroscopicity of the organic-rich phase, while above SRH, the water uptake is determined by the water-rich phase. Most likely, after LLPS the organic rich-phase includes high molecular pollen species mainly membrane proteins, starch, and lipids (Stanley and Linskens, 1974). In contrast, in the water-rich phase, the potential components are hydrophilic carbohydrates (glucose, fructose, sucrose, and maltose), water-soluble proteins, and ions (Table 1). Since the analysis of the chemical composition of SPP samples is incomplete and includes only certain classes of compounds, we used Eq. (9) to approximate non-ideal behavior of κ_b before phase separation. The obtained fit curves were extrapolated to $a_w = 1$ and are shown in panels (**b**), (**d**), (**f**) of Fig. 9. The best-fit parameters are listed in Table 4.

Table 4. Parameters characterizing the hygroscopic properties of subpollen particles with $D_{b,H\&D,min}$ ~95 nm: best-fit values (± SD) for the three-parameter fit (k_1, k_2, k_3; Eq. 9) and SRH of LLPS; n and R^2 are the number of data points and the coefficient of determination of the fit, respectively.

Species	k_1	k_2	k_3	R^2	a_w range	n	SRH (%)
Birch SPP	0.356 ± 0. 310	-0.310 ± 0.079	0.109 ± 0.049	0.937	0.55 – 0.97	66	97.7
Pine SPP	0.269 ± 0.031	-0.041 ± 0.077	-0.084 ± 0.048	0.953	0.55 – 0.96	71	98.2
Rapeseed SPP	0.291± 0.040	-0.329 ± 0.108	0.189 ± 0.072	0.672	0.55 – 0.93	31	94.6

The difference between extrapolated and measured κ_b demonstrates the effect of LLPS on the water uptake. The onset a_w of LLPS was determined as a minimum in the $\kappa_b(a_w)$ dependency ($d\kappa_b/da_w = 0$) and corresponding SRH values converted from obtained a_w of LLPS are given in Table 4. The onset SRH of the birch SPP (97.7 %) and pine SPP (98.2 %) are comparable, while the SRH of rapeseed SPP is remarkably lower (94.6 %). The SRH value depends on the dipole moment of organic material, and this parameter is a function of the elemental oxygen to carbon (O/C) ratio. Multiple experiments with organic material showed that LLPS has been observed for O/C < 0.5 and never observed for O/C > 0.8, and this rule applies to both, simple and complex mixtures (You et al., 2014). Parameterizations reported by Bertram et al. (2011) and Song et al. (2012) indicate that the SRH tends to decrease with an increasing O/C ratio. It is possible, therefore, that the lower SRH obtained for rapeseed subparticles is caused by a higher content of more oxidized organic compounds relative to birch and pine samples.

The main water active organic components of SPP are carbohydrates and proteins (Table 1). For carbohydrates the O/C ratio is close to one, therefore, it is unlikely that they can initiate LLPS. The average O/C ratio in protein-forming amino acids is 0.4; thus, proteins are suitable candidates for triggering spinodal decomposition. The SRH at that O/C ratio is in the range of 95-100% with a weak effect of organic-inorganic ratio on SRH (You et al., 2014; Bertram et al. 2011). The experimental SRH values for SPP are within 95-98%, indicating that proteins as well other organic compounds with an O/C ratio near 0.4 may be responsible for LLPS.

Dissolution of sparingly soluble organic compounds may also contribute to the hygroscopicity. Modified κ-Köhler models that assumes limited water solubility predicts a monotonic increase of κ values for an a_w increasing (Petters et al., 2009; Pajunoja et al., 2015). However, the decreasing trend of κ_b observed in the a_w range of 0.6-0.95 cannot be explained by these models (panels (**b**), (**d**), and (**f**) of Fig. 9). In addition, the solubility-based prediction is inconsistent with the size-resolved CCN measurements. As can be seen from Table 3, the growth factor ($g_a = D_{wet,a}/D_a$) at the activation point increases with an increasing D_a (decreasing S) that should results in more organic solute

dissolved in the aqueous phase, thus increasing the κ value. The CCN-derived κ_a values rather demonstrate the opposite effect (Fig. 8), that is, an increase in D_a on average leads to a decrease in κ_a. Most likely, this dependence results from the unequal composition of the dry particles, as discussed above. Taking into account the above arguments, we tend to assume that sparingly soluble compounds have little effect on the water uptake of the SPP studied.

Figure 10 shows the possible evolution of SPP morphology upon interaction with water vapor. This cartoon unites early studies with amorphous particles (Mikhailov et al., 2009; Koop et al., 2011)
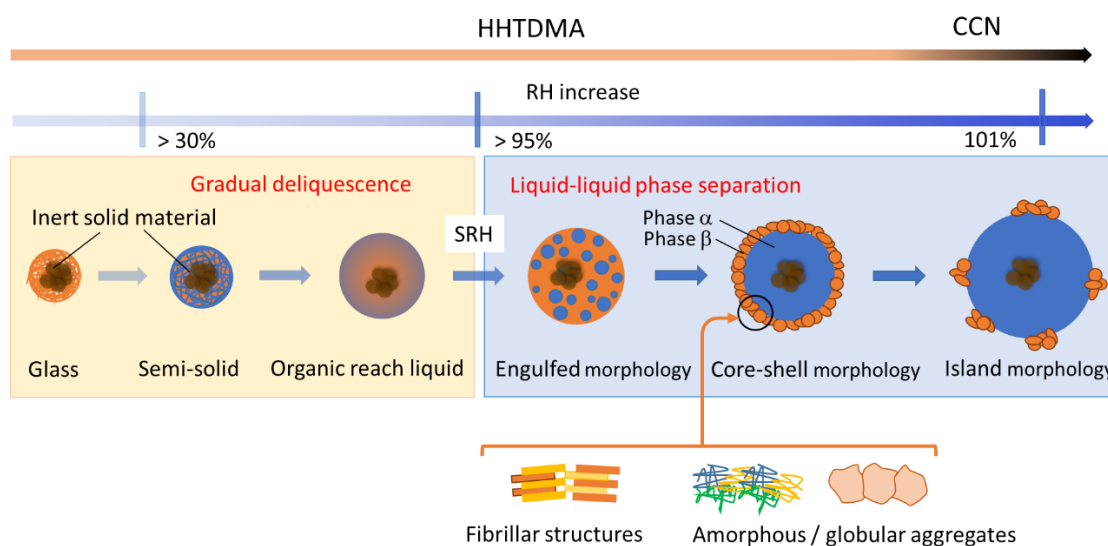
Fig. 10. Water uptake by amorphous subpollen particles: possible morphology and processes. SRH is the RH onset of liquid-liquid phase separation.

and those relatively new results associated with LLPS of multicomponent systems (Renbaum-Wolff et al., 2016; Ruehl et al., 2016; Song et al., 2017a; Ovadnevaite et al., 2017; Rastak et al., 2017). At low RH particles are in an amorphous glassy state. Due to the small diffusion coefficient of water (D_{H_2O}) in the glassy matrix (typically below $10^{-10}\,\text{cm}^2\,\text{c}^{-1}$ at 300 K) the water uptake occurs only at the particle surface. Upon further increase in RH, the outermost layers will absorb more water, which softens the matrix and act as plasticizer, thus reducing viscosity and increasing D_{H_2O}. At RH range above ~30%, particle undergo a humidity-induced phase transition from glass to a semi-solid state. This induces a self-accelerating process such that significant water uptake occurs in a gradual deliquescence process, and the semi-solid turns into organic-rich liquid. At high RH (> 95%), particles containing hydrophobic and hydrophilic organics undergo LLPS forming water-rich (α) and organic-rich (β) phases (Fig.10). The specific value of SRH is a function of O/C ratio and ions content (salting in/out effects) (You et al., 2014, and references therein). On the initial stage of LLPS, the partially engulfed morphology is preferable; with a further RH growth, the water-enriched inclusions increase in size and coagulate into one phase forming particles with core-shell morphology where the aqueous phase being mostly responsible for particle growth at high RH. Under continuing growth condition,

the organic shell will reach a relatively small volume compared to the growing volume of the aqueous core phase, such that it becomes impossible to form a complete organic shell. Under such conditions, the organic material may spread out as molecular "islands" at the surface of the core (Fig.10) (Ovadnevite et al., 2017). The transition from a coherent phase (organic film) to a spread out "gaseous" state on a 2-dimensional (2D) droplet surface can be modelled as a 2D phase transition, as described, by Ruehl et al. (2016). The presented particle morphology after LLPS (Fig.10) is based on microscopy images of supermicron samples (Renbaum-Wolff et al., 2016; Song et al., 2017a) and can differ from ~100 nm particles studied here. Our results, however, are in agreement with these images. Panels (**b**), (**d**), and (**f**) of Fig. 9 clearly show that at LLPS, water uptake does not occur instantaneously, but rather within a certain Δa_w, suggesting that a phase separation includes a sequential morphological transformation from an organic-rich phase to a water-rich phase. A similar agreement between microscopic images and the phase transition processes govern the water interactions by the 100 nm particles was observed by Rastak et al. (2017) in the case of monoterpenes derived SOA.

Insert in panels (**a**), (**c**), (**e**) of Fig. 9 shows the κ-Köhler modeling results (Eq.6) with minimum and maximum κ_b values observed on the $\kappa_b(a_w)$ dependences (panels (**b**), (**d**), (**f**) of Fig.9). The difference in the Köhler curves reflects potential uncertainty arising from spinodal decomposition. The lower Köhler curve fits the particle growth factors before onset SRH (orange line), while upper Kohler curve corresponds to maximum κ_b observed after LLPS. Intermediate data points indicate gradual phase separation accompanied by the particle engulfed morphology (Fig.10).

Figure 11 shows the hygroscopicity parameter, κ measured by HHTDMA and CCNC in SPP. The HHTDMA-derived κ_b values taken after a_w of LLPS (orange line in panels (**b**), (**d**), and (**f**) of Fig.9). One can see that within the measurement uncertainty of CCN setup, the maximum values of the HHTDMA-derived κ_b with $D_{b,H\&D,min}$ ~ 96 nm coincide with the CCN-derived κ_a with D_a ~100 nm (yellow data points) having a similar chemical composition, i.e., 0.17±0.01 vs. 0.18±0.03; 0.20±0.01 vs. 0.21±0.03; and 0.19±0.01 vs. 0.20±0.03 for birch, pine, and rapeseed SPP, respectively. Note the agreement in κ is achieved assuming that the surface tension equals σ_w, suggesting that the effect of the organic coating is negligible. One possible explanation is that the organic material establishes a partial shell covering of the water-rich phase ("island" morphology, Fig.10). Following to Ovadnevaite et al. (2017) the surface coverage parameter, c_β is

$$c_\beta = min\left[\frac{V_\beta}{V_\delta}, 1\right] ,\qquad\qquad (12)$$

where V_β is the volume of phase β and V_δ is the volume of a spherical shell of minimum thickness $\delta_{\beta,min}$, corresponding to a molecular single layer. In this study the volume of phase β was calculated

as

$$V_\beta = \frac{\pi}{6} D_{H\&D,min}^3 \times 0.07 \,, \tag{13}$$

assuming that the hydrophobic organic volume fraction in the dry particles is ~7%. This assumption is based on the chemical analysis of aqueous pollen extracts (Table 1), containing high molecular species such as protein ~3%, extractable starch ~2%, and other uncounted macromolecules ~2% (lipids, phenolic compounds, etc.). Here we assume that mass and volume fractions of pollen species are equal. Inert (surface inactive) solid material, such as cross-linking callose, sporopollenin, and cellulose is not considered (Sect. 3.1). The volume of spherical shell was derived from

$$V_\delta = \frac{4}{3} \pi \left[\left(\frac{D_{wet}}{2} \right)^3 - \left(\frac{D_{wet}}{2} - \delta_{\beta,min} \right)^3 \right] , \tag{14}$$

where $\delta_{\beta,min}$ is used as a free parameter varying from 0.4 to 5 nm. In the previous studies (Ruehl et al., 2016; Renbaum-Wolff et al., 2016; Liu et al., 2018) the $\delta_{\beta,min}$ value of 0.16 and 0.3 nm was used
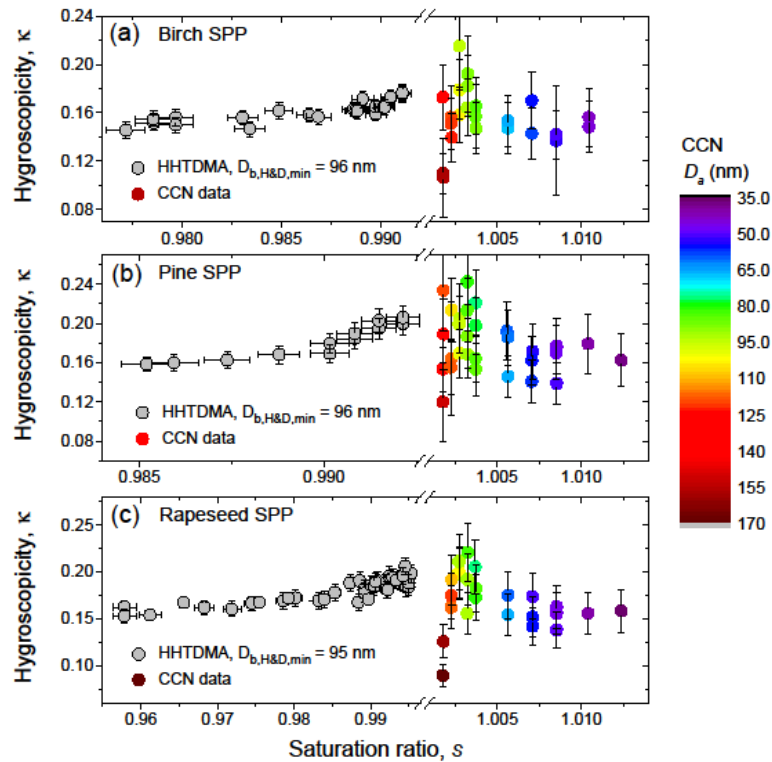
Fig. 11. HHTDMA-based and CCN-based hygroscopicity parameter, κ for birch (**a**), pine (**b**) and rapeseed (**c**) SPP as a function of RH. The color code shows the CCN-derived κ_a with respect to the shape corrected activation diameters, D_a.

for LLPS modeling of multicomponent organic mixtures with molar mass (*M*) ranging 150-360 Da (Zuend and Seinfeld, 2012). The molar mass of biomolecules and their size is significantly larger. In

particular, the M of plant proteins is mainly 0.5-500 kDa (Mohanta et al., 2019), and their volume-equivalent diameter is 2.2-10.4 nm, respectively (Erickson, 2009); therefore, we expanded the possible
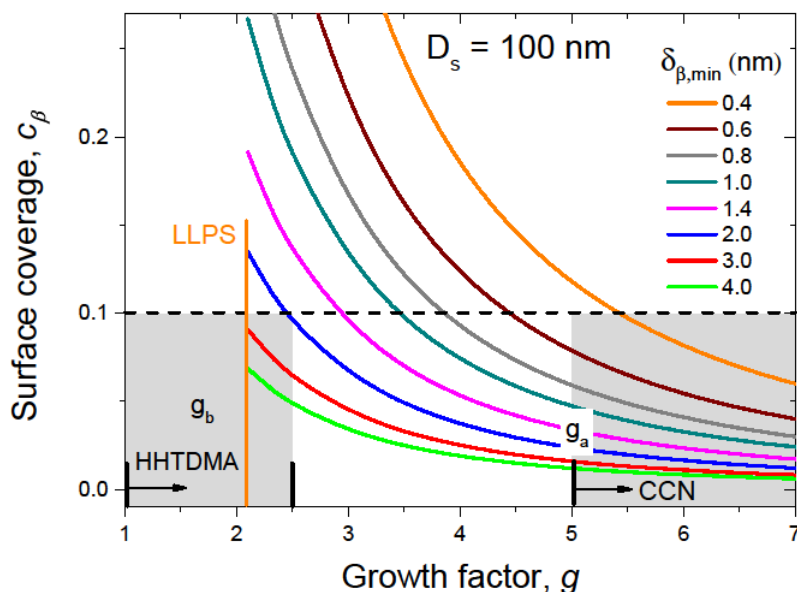
Figure 12. The surface coverage, c_β as a function of particle growth factor, $g = D_{wet}/D_s$ with D_s =100 nm, obtained for different values of the monolayer thickness, $\delta_{\beta,min}$ (colored lines). For HHTDMA and CCN measurements, D_s equals $D_{H\&D,min}$ and D_a, respectively. $g_a = D_{wet,a}/D_a$ is the growth factor at the activation diameter, $D_a \approx 100$ nm. The gray areas show the growth factor range of HHTDMA and CCN measurements. The dashed line indicates the c_β value bellow which $\sigma \approx \sigma_w$. Both g_a and g_b growth factors are average values of the birch, pine, and rapeseed samples.

range of $\delta_{\beta,min}$ up to 5 nm. The effective surface tension of the droplet, σ is calculated as the weighted mean of the composition-dependent surface tensions from α and β phases (Fig. 10):

$$\sigma = (1 - c_\beta)\sigma_\alpha + c_\beta\sigma_\beta , \qquad (15)$$

where σ_α and σ_β is the surface tension of the water-rich and organic-rich phase. Figure 12 shows the calculation results for D_s =100 nm based on Eqs. (12)-(14), which presented as $c_\beta(g = D_{wet}/D_s)$ dependences, obtained for different values of the monolayer thickness. One can see that at $\delta_{\beta,min} > 2$ nm both for the HHTDMA- and CCN-derived growth factors obtained after LLPS, the surface coverage does not exceed 0.1. Using $c_\beta = 0.1$ and assuming that the surface tension of water-rich and organic-rich phase is 72 and 57 ± 5 mNm[-1] (Absolom et al., 1981; Makievski et al., 1990; Alahverdjieva et al., 2008), respectively, it follows from Eq. (15) that σ equals 70.5 ± 0.5 mNm[-1]. That is, for particles with $D_s = 100$ nm at $\delta_{\beta,min} > 2$ due to partial shell covering (Fig.10, "island" morphology), the surface effect of biomolecules becomes negligibly small. A small contribution of

organic coating to the surface tension of the diluted droplets was also observed in CCN activation experiments with pollenkitt particles (Prisle et al., 2019).

In our simplified calculations, protein and extractable starch molecules were chosen as a main surface-active components. Depending on polarity, hygroscopicity, concentration, and electrostatic charge, this group of biomolecules can form higher-order fibrillary, globular, and amorphous aggregates, significantly affecting the thermodynamic and kinetic properties of the surface layer (Fig.10) (Lad et al., 2006; Jarpa-Parra, et al., 2015; Zapadka et al., 2017; Trainor et al.,2017; D'Imprima et al., 2019). Moreover, some biopolymers are initially prone to forming two-dimensional aggregates at the air/water interface, making the assumption of mono/multi-layer adsorption redundant (Fainerman and Miller, 1999). In addition, other organic and inorganic species present in the SPP may effect on the thermodynamic properties of the air/water interface, decreasing or increasing surface tension of the droplets (Lin and Timasheff, 1996; Fainerman et al 1998; Kotsmar et al., 2009). Additional studies are needed to specify the effect of biomolecules on the aerosol particles hygroscopic and CCN properties, including LLPS stage.

4   Summary and conclusions

In this study, we have presented measurement results of hygroscopic and cloud condensation nuclei properties of biological aerosols obtained by nebulization and drying of the birch, pine, and rapeseed pollen aqueous extracts. These studies were supplemented with chemical analysis of the pollen species, as well as gravimetric and dynamic light scattering (DLS) measurements to determine the mass fraction of hydrosols and their size distribution, respectively. The analysis results suggest that the initial dry particles in the size range of 20-190 nm are a mixture of different proportions of water-soluble and water-insoluble compounds. The analysed fraction of water-extractable biomolecules includes proteins and starch. Among the water-soluble compounds, the main ones are inorganic ions and monosaccharides. Aqueous extracts contain also a significant amount of water-insoluble species (~50 wt %) which are mainly in the size range of 20-80 nm.

The HHTDMA studies in the H&D (restructuring) mode have shown that the DMA1 selected particles ranging 30-180 nm have a porous structure wherein the void fraction gradually increases with size, reaching ~26% for 180 nm birch and pine SPP. The minimum mobility diameters obtained in H&D mode were used as a proxy of the mass equivalent diameters of the initial dry particles.

CCN measurements revealed that the shape corrected dry activation diameters measured at S = 0.18-1.24 % are in the range of 137-44 nm, 134-38 nm, and 159-38 nm for birch, pine and rapeseed SPP, respectively. For all samples at high S (> 0.6%), the maximum activated fraction is generally well below one, and heterogeneity range ($\sigma_a/D_{b,a}$) reaching up to 30-40 %. Both indicate a substantial fraction of CCN-inactive particles with low hygroscopicity. A weak but noticeable size-dependent

variation in κ was observed, ranging from 0.13-0.18, 0.16-0.20, and 0.12-0.20, for birch, pine and rapeseed SPP, respectively. For all SPP studied the maximum κ values refer to D_a = 80-120 nm, and low values correspond to particles with activation diameters below and above this size range. Most likely, particles with $D_a < 80$ nm are enriched in primary non-hygroscopic colloids, while particles with $D_a > 120$ nm may contain their aggregates.

The sensitivity analysis of the CCN results has shown that the uncertainty in hygroscopicity parameter, $\delta\kappa$ caused by irregular particle morphology is strongly dependent on their size, increasing from 4 % to 25 % with particle size increases from 30 nm to 160 nm, respectively. In general, the CCN measurement results show that the SPP at sizes exceeding 45 nm are CCN-active at supersaturations less than 1 % and, therefore, can participate in the formation and modification of cloud systems.

The hygroscopic properties of SPP with $D_{H\&D,min}$~ 96 nm were investigated by the high humidity tandem differential mobility analyser (HHTDMA) ranging 2 - 99.5 % RH. Over the entire RH range, the water uptake of SPP occurred gradually and reversibly, similar to the behavior of amorphous organic substances. A significant amount of absorbed water (g_b >1.4) was observed at RH > 95 %, with further RH increasing (RH > 97%), particle uptake more water leading to an abrupt increase in the growth factors: approximately ~1% RH results in a 3-fold increase in the particle volume. Due to the solution non-ideality, the HHTDMA-derived hygroscopicity parameter, κ exhibits a decreasing trend in the 0.6-0.95 a_w range and sharp increases at $a_w > 0.95$. We suggest that the observed $g(RH)$ and $\kappa_b(a_w)$ dependences at high RH are the result of liquid-liquid phase separation of the multicomponent SPP. For birch, pine and rapeseed subpollen particles, the onset RH of LLPS was estimated to be 97.7%, 98.2%, and 94.6%, respectively.

A good agreement in κ was obtained between HHTDMA at RH > 97 % and CCN-derived values. We believe that this closure became possible by the extended upper limit in RH of our HHTDMA system (up to 99.5%). Discrepancy between the κ, measured below and above water saturation in the organic and organic-inorganic mixed particles have been reported in several studies (Song et al., 2017a; Zhao et al., 2016; Hansen et al., 2015; Pajunoja et al., 2015; Whitehead et al., 2014; Alfarra et al., 2013; Dusek et al., 2011; Massoli et al., 2010, Good et al., 2010). Petters et al. (2006), Hodas et al. (2016), Renbaum-Wolf et al., (2016), Rastak et al. (2017), and Liu et al. (2018) suggested that such discrepancies are expected in systems that undergo LLPS at high RH. Usually, the CCN-derived κ values are compared with those obtained by the HTDMA at RH < 95 %, which leads to their discrepancy, especially for the organic particles with low O/C ratio (Song et al., 2017a). In this study, the growth factors were also measured at RH above LLPS so that both HHTDMA and CCN measurements provides the κ values of the water-rich phase, which enabled us to close the gap between the particle's hygroscopic growth and their CCN activation. The closure between HHTDMA- and

CCN-derived κ was achieved when the value of σ was that of water, suggesting that above LLPS, due to large growth factors, the surface-active biomolecules are not able to fully coat the water-rich phase. Most likely, an "islands" composed of 2D or 3D aggregates at the air-water interface are forming.

In conclusion, the obtained and discussed hygroscopic and CCN properties of the SPP, including spinodal decomposition, may be common for atmospheric particles, such as natural sea-spray (Ovadnevaite et al., 2011; Estillore et al., 2017; Lee et al., 2020) and rainforest aerosols (Simoneit et al., 1990; Graham et al., 2003 and Pöschl et al.2010) as well as anthropogenic aerosols, containing a broad spectrum of biopolymers coupled with water-soluble organic and inorganic material in different proportions (Xu et al., 2020; Song et al., 2017b; Fröhlich-Nowoisky et al., 2016; Pöschl and Shiraiwa, 2015; You et al., 2014; Pöhlker et al., 2012; Schneider et al., 2011; Graber and Rudich, 2006; Zhang and Anastasio, 2003).   In addition, the ability of SPP undergo LLPS at subsaturated conditions forming a water-rich phase may enhance post-translational modifications of the proteins induced by air pollutants (O_3, NO_2) and therefore reinforce their allergic potential. This information may be useful for prognostic assessments of allergic diseases such as thunderstorm asthma (Suphioglu, 1998; Pöschl et al., 2015; Reinmuth-Selzle et al., 2017; Beggs, 2017; Kornei, 2018; Yair et al., 2019, Hughes at al., 2020).

Data availability. The data presented in this article can be accessed through the corresponding author Eugene Mikhailov (eugene.mikhailov@spbu.ru).

Supplement

Author contributions. EFM designed the study, performed the concomitant measurements, and wrote this paper, MLP, LAK, and OOK conducted the CCN measurements, KR-S and JF-N conducted the chemical analyses, AAK., OAI, SSV, CP, and UP contributed to the discussion of the results.

Competing interests. The authors declare that they have no conflict of interest.

Acknowledgements. We thank the Geomodel Research Center, Interdisciplinary Resource Center for Nanotechnology, Chemical Analysis and Materials Research Centre and Center for Optical and Laser Methods of Matter Research at Saint Petersburg State University. We also thank Mohammed Katzia for technical support in the course of the CCN measurements.

Financial support. This research has been supported by the Russian Science Foundation (grant no. 18-17-00076) and Max Planck Society.

References

Absolom, D. R., Van Oss, C. J., Zingg, W., and Neumann, A. W.: II. Surface tension of serum albumin, altered at the protein-air interface Biochim. Biophys. Acta, 670, 74-78, https://doi.org/10.1016/0005-2795(81)90050-7, 1981.

Alahverdjieva, V. S., Fainerman, V. B., Aksenenko, E. V., Leser, M. E., and Miller, R.: Adsorption of hen egg-white lysozyme at the air–water interface in presence of sodium dodecyl

sulphate, Colloids Surf. A Physicochem. Eng. Asp., 317, 610-617, https://doi.org/10.1016/j.colsurfa.2007.11.062, 2008.

Alfarra, M. R., Good, N., Wyche, K. P., Hamilton, J. F., Monks, P. S., Lewis, A. C., and McFiggans, G.: Water uptake is independent of the inferred composition of secondary aerosols derived from multiple biogenic VOCs, Atmos. Chem. Phys., 13, 11769–11789, https://doi.org/10.5194/acp-13-11769-2013, 2013.

Andreae, M. O. and Rosenfeld, D.: Aerosol-cloud-precipitation interactions. Part 1. The nature and sources of cloud-active aerosols, Earth-Sci. Rev., 89, 13–41, https://doi.org/10.1016/j.earscirev.2008.03.001, 2008.

Augustin, S., Wex, H., Niedermeier, D., Pummer, B., Grothe, H., Hartmann, S., Tomsche, L., Clauss, T., Voigtländer, J., Ignatius, K., and Stratmann, F.: Immersion freezing of birch pollen washing water, Atmos. Chem. Phys., 13, 10989–11003, https://doi.org/10.5194/acp-13-10989-2013, 2013.

Baker, H. G., and Baker, I.: Starch in angiosperm pollen grains and its evolutionary significance. Am. J. Bot., 66, 591-600, https://doi.org/10.1002/j.1537-2197.1979.tb06262.x, 1979.

Beggs, P. J.: Allergen aerosol from pollen-nucleated precipitation: A novel thunderstorm asthma trigger, Atmos. Environ., 152, 455-457, https://doi.org/10.1016/j.atmosenv.2016.12.045, 2017.

Bertram, A. K., Martin, S. T., Hanna, S. J., Smith, M. L., Bodsworth, A., Chen, Q., Kuwata, M., Liu, A., You, Y., and Zorn, S. R.: Predicting the relative humidities of liquid-liquid phase separation, efflorescence, and deliquescence of mixed particles of ammonium sulfate, organic material, and water using the organic-to-sulfate mass ratio of the particle and the oxygen-to-carbon elemental ratio of the organic component, Atmos. Chem. Phys., 11, 10995–11006, https://doi.org/10.5194/acp-11-10995-2011, 2011.

Biskos, G., Paulsen, D., Russell, L. M., Buseck, P. R., and Martin, S. T.: Prompt deliquescence and efflorescence of aerosol nanoparticles, Atmos. Chem. Phys., 6, 4633–4642, https://doi.org/10.5194/acp-6-4633-2006, 2006.

Brockmann, J. E. and Rader, D. J.: APS response to nonspherical particles and experimental determination of dynamic shape factor, Aerosol Sci. Technol., 13, 162–172, https://doi.org/10.1080/02786829008959434, 1990.

Chen, J.-P., Hazra, A., and Levin, Z.: Parameterizing ice nucleation rates using contact angle and activation energy derived from laboratory data, Atmos. Chem. Phys., 8, 7431–7449, https://doi.org/10.5194/acp-8-7431-2008, 2008.

Chen, L., Chen, Y., Chen, L., Gu, W., Peng, C., Luo, S., Song, W., Wang, Z., and Tang, M.: Hygroscopic properties of 11 pollen species in China, ACS Earth Space Chem., 3(12), 2678-2683, https://doi.org/ 10.1021/acsearthspacechem.9b00268, 2019.

Cheng, Y. F., Wiedensohler, A., Eichler, H., Heintzenberg, J., Tesche, M., Ansmann, A., Wendisch, M., Su, H., Althausen, D., Herrmann, H., Gnauk, T., Bruggemann, E., Hu, M., and Zhang, Y. H.: Relative humidity dependence of aerosol optical properties and direct radiative forcing in the surface boundary layer at Xinken in Pearl River Delta of China: An observation based numerical study, Atmos. Environ., 42, 6373–6397, https://doi.org/10.1016/j.atmosenv.2008.04.009, 2008.

Chichiriccò, G., Pacini, E., and Lanza, B.: Pollenkitt of some monocotyledons: lipid composition and implications for pollen germination, Plant. Biol., 21, 920-926, https://doi.org/10.1111/plb.12998, 2019.

DeCarlo, P. F., Slowik, J. G., Worsnop, D. R., Davidovits, P., and Jimenez, J. L.: Particle morphology and density characterization by combined mobility and aerodynamic diameter measurements. Part 1: Theory, Aerosol Sci. Technol., 38, 1185–1205, https://doi.org/10.1080/027868290903907, 2004.

Diehl, K., Quick, C., Matthias-Maser, S., Mitra, S. K., and Jaenicke, R.: The ice nucleating ability of pollen – Part I: Laboratory studies in deposition and condensation freezing modes, Atmos. Res., 58, 75–87, https://doi.org/10.1016/S0169-8095(01)00091-6, 2001.

Diehl, K., Matthias-Maser, S., Jaenicke, R., and Mitra, S. K.: The ice nucleating ability of pollen: Part II. Laboratory studies in immersion and contact freezing modes, Atmos. Res., 61, 125–133, doi:10.1016/s0169-8095(01)00132-6, 2002.

Després, V. R., Huffman, J. A., Burrows, S. M., Hoose, C., Safatov, A. S., Buryak, G., Fröhlich-Nowoisky, J., Elbert, W., Andreae, M. O., Pöschl, U., and Jaenicke, R.: Primary biological aerosol particles in the atmosphere: a review, Tellus B, 64, 15598, https://doi.org/10.3402/tellusb.v64i0.15598, 2012.

D'Imprima, E., Floris, D., Joppe, M., Sànchez, R., Grininger, M., and Kühlbrandt, W.: Protein denaturation at the air-water interface and how to prevent it, eLife, 8, e42747, https://doi.org/10.7554/eLife.42747.001, 2019.

Dusek, U., Frank, G. P., Massling, A., Zeromskiene, K., Iinuma, Y., Schmid, O., Helas, G., Hennig, T., Wiedensohler, A., and Andreae, O. M.: Water uptake by biomass burning aerosol at sub- and supersaturated conditions: closure studies and implications for the role of organics, Atmos. Chem. Phys., 11, 9519–9532, https://doi.org/10.5194/acp-11-9519-2011, 2011.

Erickson, H. P.: Size and Shape of Protein Molecules at the Nanometer Level Determined by Sedimentation, Gel Filtration, and Electron Microscopy, Biol. Priced. Online, 11, 32-51, https://doi.org/10.1007/s12575-009-9008-x, 2009.

Estillore, A. D., Morris, H. S., Or, V. W., Lee, H. D., Alves, M. R., Marciano, M. A., Laskina, O., Qin, Z., Tivanski, A. V., and Grassian, V. H.: Linking hygroscopicity and the surface microstructure of model inorganic salts, simple and complex carbohydrates, and authentic sea spray aerosol particles, Phys. Chem. Chem. Phys., 19, 21101-21111, https://doi.org/10.1039/C7CP04051B, 2017.

Fainerman, V. B., and Miller, R.: Equation of State for Concentrated Protein Surface Layers at the Water/Air Interface, Langmuir, 15, 1812-1816, https://doi.org/10.1021/la981180h, 1999.

Fainerman, V. B., Lucassen-Reynders, E. H., and Mller, R.: Adsorption of surfactants and proteins at fluid interfaces, Colloids Surf. B, 143, 141-165, https://doi.org/10.1016/S0927-7757(98)00585-8, 1998.

Fröhlich-Nowoisky, J., Kampf, C. J., Weber, B., Huffman, A., Pöhlker, C., Andreae, M. O., Hoor, P., Thines, E., Hoffman. T., Després, V. R., and Pöschl, U.: Bioaerosols in the Earth system: Climate, health, and ecosystem interactions, Atmos. Res., 182, 346-476, https://doi.org/10.1016/j.atmosres.2016.07.018, 2016.

Good, N., Topping, D. O., Duplissy, J., Gysel, M., Meyer, N. K., Metzeger, A., Turner, S. F., Baltensperger, U., Ristovski, Z., Weingartner, E., Coe, H., and McFiggans, G.: Widening the gap between measurement and modelling of secondary organic aerosol properties?, Atmos. Chem. Phys., 10, 2577–2593, https://doi.org/10.5194/acp-10-2577-2010, 2010.

Graber, E. R. and Rudich, Y.: Atmospheric HULIS: How humic-like are they? A comprehensive and critical review, Atmos. Chem. Phys., 6, 729–753, https://doi.org/10.5194/acp-6-729-2006, 2006.

Graham, B., Guyon, P., Taylor, P. E., Artaxo, P., Maenhaut, W., Glovsky, M. M., Flagan, R. C., and Andreae, M. O.: Organic compounds present in the natural Amazonian aerosol: Characterization by gas chromatography–mass spectrometry, J. Geophys. Res., 108(D24), 4766, https://doi.org/10.1029/2003JD003990, 2003.

Griffiths, P. T., Borlace, J. S., Gallimore, P. J., Kalberer, M., Herzog, M., and Pope, F. D.: Hygroscopic growth and cloud activation of pollen: a laboratory and modelling study, Atmos. Sci. Lett., 13, 289–295, https://doi.org/10.1002/asl.397, 2012.

Grote, M., Vrtala, S., Niederberger, V., Wiermann, R., Valenta, R., and Reichelt, R.: Release of allergen-bearing cytoplasm from hydrated pollen: A mechanism common to a variety of grass (Poaceae) species revealed by electron microscopy, J. Allergy Clin. Immunol., 108, 109-115, https://doi.org/10.1067/mai.2001.116431, 2001.

Grote, M., Valenta, R., and Reichelt, R.: Abortive pollen germination: A mechanism of allergen release in birch, alder, and hazel revealed by immunogold electron microscopy. J. Allergy Clin. Immunol., 111, 1017–1023, https://doi.org/10.1067/mai.2003.1452, 2003.

Gysel, M., Weingartner, E., Nyeki, S., Paulsen, D., Baltensperger, U., Galambos, I., and Kiss, G.: Hygroscopic properties of water-soluble matter and humic-like organics in atmospheric fine aerosol, Atmos. Chem. Phys., 4, 35–50, https://doi.org/10.5194/acp-4-35-2004, 2004.

Hansen, A. M. K., Hong, J., Raatikainen, T., Kristensen, K., Ylisirniö, A., Virtanen, A., Petäjä, T., Glasius, M., and Prisle, N. L.: Hygroscopic properties and cloud condensation nuclei activation of limonene-derived organosulfates and their mixtures with ammonium sulfate, Atmos. Chem. Phys., 15, 14071–14089, https://doi.org/10.5194/acp-15-14071-2015, 2015.

Hänel, G.: The properties of atmospheric aerosol particles as function of relative humidity at the thermodynamic equilibrium with surrounding moist air, Adv. Geophys. 19, 73–188, https://doi.org/10.1016/S0065-2687(08)60142-9, 1976.

Hodas, N., Zuend, A., Schilling, K., Berkemeier, T., Shiraiwa, M., Flagan, R. C., and Seinfeld, J. H.: Discontinuities in hygroscopic growth below and above water saturation for laboratory surrogates of oligomers in organic atmospheric aerosols, Atmos. Chem. Phys., 16, 12767–12792, https://doi.org/10.5194/acp-16-12767-2016, 2016.

Hoose, C., Kristjansson, J. E., and Burrows, S. M.: How important is biological ice nucleation in clouds on a global scale? Environ. Res. Lett., 5, 1–7, doi:10.1088/1748-9326/5/2/024009, 2010.

Hoose, C. and Möhler, O.: Heterogeneous ice nucleation on atmospheric aerosols: a review of results from laboratory experiments, Atmos. Chem. Phys., 12, 9817–9854, https://doi.org/10.5194/acp-12-9817-2012, 2012.

Huffman, J. A., Prenni, A. J., DeMott, P. J., Pöhlker, C., Mason, R. H., Robinson, N. H., Fröhlich-Nowoisky, J., Tobo, Y., Després, V. R., Garcia, E., Gochis, D. J., Harris, E., Müller-Germann, I., Ruzene, C., Schmer, B., Sinha, B., Day, D. A., Andreae, M. O., Jimenez, J. L., Gallagher, M., Kreidenweis, S. M., Bertram, A. K., and Pöschl, U.: High concentrations of biological aerosol particles and ice nuclei during and after rain, Atmos. Chem. Phys., 13, 6151–6164, https://doi.org/10.5194/acp-13-6151-2013, 2013.

Hughes, D. D., Mampage, B. A., Jones, L. M., Liu, Z., and Stone, E. A.: Characterization of atmospheric pollen fragments during springtime thunderstorms, Environ. Sci. Technol. Lett., 7, 409−414, https://doi.org/10.1021/acs.estlett.0c00213, 2020.

Koop, T., Bookhold, J., Shiraiwa, M., and Pöschl, U.: Glass transition and phase state of organic compounds: dependency on molecular properties and implications for secondary organic aerosols in the atmosphere, Phys. Chem. Chem. Phys., 13, 19238–19255, https://doi.org/10.1039/C1CP22617G, 2011.

Kornei, K.: Australian state forecasts deadly thunderstorm asthma, Science, 359 (6374), 380, https://doi.org/10.1126/science.359.6374.380, 2018.

Kotsmar, Cs., Pradines, V., Alahverdjieva, V. S., Aksenenko E.v., Fainerman, V. B., Kovalchuk, V. I., Krägel, J., Leser, M. E., Noskov, B. A., and Miller, R.: Thermodynamics, adsorption kinetics and rheology of mixed protein–surfactant interfacial layers, Adv. Colloid Interface Sci., 150, 41-54, https://doi.org/10.1016/j.cis.2009.05.002, 2009.

Kreidenweis, S. M., Koehler, K., DeMott, P. J., Prenni, A. J., Carrico, C., and Ervens, B.: Water activity and activation diameters from hygroscopicity data – Part I: Theory and application to inorganic salts, Atmos. Chem. Phys., 5, 1357–1370, https://doi.org/10.5194/acp-5-1357-2005, 2005.

Kuparinen, A., Katul, G., Nathan, R., and Schurr, F. M.: Increases in air temperature can promote wind-driven dispersal and spread of plants, Proc. Roy. Soc. B-Biol. Sci., 276, 3081–3087, http://doi.org/10.1098/rspb.2009.0693, 2009.

Lad, M. D., Birembout, F., Mattew, J. M., Frazier, R. A., and Green, R.J.: The adsorbed conformation of globular proteins at the air/water interface, Phys. Chem. Chem. Phys., 8, 2179-2186, https://doi.org/10.1039/b515934b, 2006.

Laurence, A. R., Thomas, A. V., Bryant, V. M., and McDonough, C.: Airborne starch granules as a potential contamination source at archaeological sites. J. Ethnobiol. 31, 213-232, https://doi.org/10.2993/0278-0771-31.2.213, 2011.

Lee, H. D., Morris, H.S., Laskina, O., Sultana, C. M., Lee, C., Jayarathne, T., Cox, J. L., Wang, X., Hasenecz, E. S., DeMott, P. J., Bertram, T. H., Cappa, C. D., Stone, E. A., Prather, K. A., Grassian, V. H., and Tivanski, A. V.: Organic enrichment, physical phase state, and surface tension depression of nascent core−shell sea spray aerosols during two phytoplankton blooms, ACS Earth Space Chem., 4, 650−660, https://dx.doi.org/10.1021/acsearthspacechem.0c00032, 2020.

Lin, T.-Y., Timasheff, S. N.: On the role of surface tension in the stabilization of globular proteins, Protein Sci., 5, 372-381, https://doi.org/10.1002/pro.55600502221996, 1996.

Liu, F., Lakey, P. S. J., Berkmeier, T., Tong, H., Kunert, A. N., Meusel., H., Cheng, Y., Su, H., Fröhlich-Nowoisky, J., Lai, S., Weller, M. G., Shiraiwa, M., Pöschl, U., and Kampf, C. J.: Atmospheric protein chemistry influenced by anthropogenic air pollutants: nitration and oligomerization upon exposure to ozone and nitrogen dioxide, Faraday Discuss., 200, 413-427, https://doi.org/10.1039/C7FD00005G, 2017

Liu, P., Song, M., Zhao, T., Gunthe, S. S., Ham, S., He, Y., Qin, Y. M., Gong, Z., Amorim, J. C., Bertram, A. K., and Martin, S. N.: Resolving the mechanisms of hygroscopic growth and cloud condensation nuclei activity for organic particulate matter. Nat. Commun. 9, 4076, https://doi.org/10.1038/s41467-018-06622-2, 2018

Jarpa-Parra, M., Bamdad, F., Tian, Z., Zeng, H., Temelli, F., and Chen L.: Impact of pH on molecular structure and surface properties of lentillegumin-like protein and its application as foam stabilizer, Colloids Surf. B, 45-53, 132, https://doi.org/10.1016/j.colsurfb.2015.04.065, 2015.

Makievski, A.V., Loglio, G., Krägel, J., Miller, R., Fainerman, V .B., and Neumann, A. W.: Adsorption of protein layers at the water/air interface as studied by axisymmetric drop and bubble shape analysis, J. Chem. Phys., 103, 9557-9561, https://doi.org/10.1021/jp990775y, 1999.

Massoli, P., Lamber, A. T., Ahern, A. T., Williams, L. R., Ehn, M., Mikkilä, J., Canagaratna, M. R., Brune, W. H., Onasch, T. B., Jayne, J. T., Petäjä, T., Kulmala, M., Laaksonen, A., Kolb, C. E., Davidovits, P., and Worsnop, D. R.: Relationship between aerosol oxidation level and hygroscopic properties of laboratory generated secondary organic aerosol (SOA) particles, Geophys. Res. Lett., 37, L24801, https://doi.org/10.1029/2010GL045258, 2010.

Masuko, T., Minami, A., Iwasaki, N., Majima, T., Nishimura, S.-I., and Lee, Y. C.: Carbohydrate analysis by a phenol–sulfuric acid method in microplate format, Anal. Biochem., 339, 69-72, https://doi.org/10.1016/j.ab.2004.12.001, 2005.

McFiggans, G., Artaxo, P., Baltensperger, U., Coe, H., Facchini, M. C., Feingold, G., Fuzzi, S., Gysel, M., Laaksonen, A., Lohmann, U., Mentel, T. F., Murphy, D. M., O'Dowd, C. D., Snider, J. R., and Weingartner, E.: The effect of physical and chemical aerosol properties on warm cloud droplet activation, Atmos. Chem. Phys., 6, 2593–2649, https://doi.org/10.5194/acp-6-2593-2006, 2006.

Mikhailov, E., Vlasenko, S., Niessner, R., and Pöschl, U.: Interaction of aerosol particles composed of protein and salts with water vapor: hygroscopic growth and microstructural rearrangement, Atmos. Chem. Phys., 4, 323–350, https://doi.org/10.5194/acp-4-323-2004, 2004.

Mikhailov, E., Vlasenko, S., Martin, S. T., Koop, T., and Pöschl, U.: Amorphous and crystalline aerosol particles interacting with water vapor: conceptual framework and experimental evidence for restructuring, phase transitions and kinetic limitations, Atmos. Chem. Phys., 9, 9491–9522, https://doi.org/10.5194/acp-9-9491-2009, 2009.

Mikhailov, E., Vlasenko, S., Rose, D., and Pöschl, U.: Mass-based hygroscopicity parameter interaction model and measurement of atmospheric aerosol water uptake, Atmos. Chem. Phys., 13, 717–740, https://doi.org/10.5194/acp-13-717-2013, 2013.

Mikhailov, E. F., Ivanova, O. A., Nebosko, E. Yu., Vlasenko, S. S., and Ryshkevich, T. I.: Subpollen particles as atmospheric cloud condensation nuclei, Izv. Atmos. Ocean Phys., 55, 357-364, https://doi.org/ 10.1134/S000143381904008X, 2019.

Mikhailov, E. F. and Vlasenko, S. S.: High-humidity tandem differential mobility analyzer for accurate determination of aerosol hygroscopic growth, microstructure, and activity coefficients over a wide range of relative humidity, Atmos. Meas. Tech., 13, 2035–2056, https://doi.org/10.5194/amt-13-2035-2020, 2020.

Mohanta, T. K., Khan, A., Hashem, A., Abd_Allah, E. F., and Al-Harrasi, A.: The molecular mass and isoelectric point of plant proteomes, BMC Genomics, 20, 631, https://doi.org/10.1186/s12864-019-5983-8, 2019.

Möhler, O., DeMott, P. J., Vali, G., and Levin, Z.: Microbiology and atmospheric processes: the role of biological particles in cloud physics, Biogeosciences, 4, 1059–1071, https://doi.org/10.5194/bg-4-1059-2007, 2007.

Morris, C. E., Conen, F., Huffman, J. A., Phillips, V., Pöschl, U., and Sands, D. C.: Bioprecipitation: A feedback cycle linking earth history, ecosystem dynamics and land use through biological ice nucleators in the atmosphere. Global Change Biology, 20, 341–351. https://doi.org/10.1111/gcb.12447, 2014.

O′Sullivan, D., Murray, B., Ross, J., Whale, T. F., Price, H. C., Atkinson, J. D., Umo, n. S., and Webb, M. E.:The relevance of nanoscale biological fragments for ice nucleation in clouds. Sci. Rep., 5, 8082, https://doi.org/10.1038/srep08082, 2015.

Ovadnevaite, J., Ceburnis, D., Martucci, G., Bialek, J., Monahan, C., Rinaldi, M., Facchini, M. C., Berresheim, H., Worsnop, D. R., and O'Dowd, C.: Primary marine organic aerosol: A dichotomy of low hygroscopicity and high CCN activity, 38, L21806, https://doi.org/10.1029/2011GL048869, 2011.

Ovadnevaite, J., Zuend, A., Laaksonen, A., Sanchez, K. J., Roberts, G., Ceburnis, D., Decesari, S., Rinaldi, M., Hodas, N., Facchini, M. C., Seinfeld, J. H., and O' Dowd, C.: Surface tension prevails over solute effect in organic-influenced cloud droplet activation, Nature, 546, 637–641, https://doi.org/10.1038/nature22806, 2017.

Pacini, T., Franchi, G. G., and Ripaccioli, M.: Ripe pollen structure and histochemistry of some gymnosperms, Pl. Syst. Evol., 217, 81-99, https://doi.org/10.1007/BF00984923, 1999.

Pacini, E. and Hesse, M.: Pollenkitt – its composition, forms and functions, Flora, 200, 399-415, https://doi.org/10.1016/j.flora.2005.02.006, 2005.

Pajunoja, A., Lambe, A. T., Hakala, J., Rastak, N., Cummings, M. J., Brogan, J. F., Hao, L. Q., Paramonov, M., Hong, J., Prisle, N. L., Malila, J., Romakkaniemi, S., Lehtinen, K. E. J., Laaksonen, A., Kulmala, M., Massoli, P., Onasch, T. B., Donahue, N. M., Riipinen, I., Davidovits, P., Worsnop, D. R., Petäjä, T., and Virtanen, A.: Adsorptive uptake of water by semisolid secondary organic aerosols, Geophys. Res. Lett., 42, 3063–3068, https://doi.org/10.1002/2015gl063142, 2015.

Petters, M. D., Kreidenweis, S. M., Snider, J. R., Koehler, K. A., Wang, Q., Prenni, A. J., and Demott, P. J.: Cloud droplet activation of polymerized organic aerosol, Tellus B, 58, 196–205, https://doi.org/10.1111/j.1600-0889.2006.00181.x, 2006.

Petters, M. D. and Kreidenweis, S. M.: A single parameter representation of hygroscopic growth and cloud condensation nucleus activity, Atmos. Chem. Phys., 7, 1961–1971, https://doi.org/10.5194/acp-7-1961-2007, 2007.

Petters, M. D., Wex, H., Carrico, C. M., Hallbauer, E., Massling, A., McMeeking, G. R., Poulain, L., Wu, Z., Kreidenweis, S. M., and Stratmann, F.: Towards closing the gap between hygroscopic growth and activation for secondary organic aerosol – Part 2: Theoretical approaches, Atmos. Chem. Phys., 9, 3999–4009, https://doi.org/10.5194/acp-9-3999-2009, 2009.

Piffanelli, P., Ross, J. H. E., and Murphy, D. J.: Biogenesis and function of the lipidic structures of pollen grains, Sex. Plant Reprod., 11, 65–80, https://doi.org/10.1007/s004970050122, 1998.

Pöhlker, C., Wiedemann, K. T., Sinha, B., Shiraiwa, M., Gunthe, S. S., Smith, M., Su, H., Artaxo, P., Chen, Q., Cheng, Y. F., Elbert, W., Gilles, M. K., Kilcoyne, A. L. D., Moffet, R. C., Weigand, M., Martin, S. T., Pöschl, U., and Andreae, M. O.: Biogenic potassium salt particles as seeds for secondary organic aerosol in the Amazon, Science, 337, 1075–1078, https://doi.org/10.1126/science.1223264, 2012.

Pöhlker, M. L., Pöhlker, C., Ditas, F., Klimach, T., Hrabe de Angelis, I., Araújo, A., Brito, J., Carbone, S., Cheng, Y., Chi, X., Ditz, R., Gunthe, S. S., Kesselmeier, J., Könemann, T., Lavric, J. V., Martin, S. T., Mikhailov, E., Moran-Zuloaga, D., Rose, D., Saturno, J., Su, H., Thalman, R., Walter, D., Wang, J., Wolff, S., Barbosa, H. M. J., Artaxo, P., Andreae, M. O., and Pöschl, U.: Long- term observations of cloud condensation nuclei in the Amazon rain forest – Part 1: Aerosol size distribution, hygroscopicity, and new model parametrizations for CCN prediction, Atmos. Chem. Phys., 16, 15709–15740, https://doi.org/10.5194/acp-16-15709-2016, 2016.

Pöhlker, M. L., Ditas, F., Saturno, J., Klimach, T., Hrabě de Angelis, I., Araùjo, A. C., Brito, J., Carbone, S., Cheng, Y., Chi, X., Ditz, R., Gunthe, S. S., Holanda, B. A., Kandler, K., Kesselmeier, J., Könemann, T., Krüger, O. O., Lavrič, J. V., Martin, S. T., Mikhailov, E., Moran-Zuloaga, D., Rizzo, L. V., Rose, D., Su, H., Thalman, R., Walter, D., Wang, J., Wolff, S., Barbosa, H. M. J., Artaxo, P., Andreae, M. O., Pöschl, U., and Pöhlker, C.: Long-term observations of cloud condensation nuclei

over the Amazon rain forest – Part 2: Variability and characteristics of biomass burning, long-range transport, and pristine rain forest aerosols, Atmos. Chem. Phys., 18, 10289–10331, https://doi.org/10.5194/acp-18-10289-2018, 2018.

Pope, F. D.: Pollen grains are efficient cloud condensation nuclei, Environ. Res. Lett., 5, 044015, https://doi.org/10.1088/1748-9326/5/4/044015, 2010.

Pöschl, U.: Atmospheric aerosols: composition, transformation, climate and health effects, Angew. Chem.-Int. Edit., 44, 7520–7540, https://doi.org/10.1002/anie.200501122, 2005.

Pöschl, U., Martin, S. T., Sinha, B., Chen, Q., Gunthe, S. S., Huffman, J. A., Borrmann, S., Farmer, D. K., Garland, R. M., Helas, G., Jimenez, J. L., King, S. M., Manzi, A., Mikhailov, E., Pauliquevis, T., Petters, M. D., Prenni, A. J., Roldin, P., Rose, D., Schneider, J., Su, H., Zorn, S. R., Artaxo, P., and Andreae, M. O.: Rainforest Aerosols as Biogenic Nuclei of Clouds and Precipitation in the Amazon, Science, 329, 1513–1516, https://doi.org/10.1126/science.1191056, 2010.

Pöschl, U. and Shiraiwa, M.: Multiphase chemistry at the atmosphere–biosphere interface influencing climate and public health in the Anthropocene, Chem. Rev., 115, 4440-4475, https://doi.org/10.1021/cr500487s, 2015.

Prenni, A. J., Tobo, Y., Garcia, E., DeMott, P. J., Huffman, J. A., McCluskey, C. S., Kreidenweis, S.M., Prenni, J. E., Pöhlker, C., and Pöschl, U.: The impact of rain on ice nuclei populations at a forested site in Colorado, Geophys. Res. Lett., 40, 227–231, https://doi.org/10.1029/2012GL05395, 2013.

Prisle, N. L., Lin, J. J., Purdue, S., Lin, H., Meredith, J. C., and Nenes, A.: Cloud condensation nuclei activity of six pollenkitts and the influence of their surface activity, Atmos. Chem. Phys., 19, 4741–4761, https://doi.org/10.5194/acp-19-4741-2019, 2019.

Pummer, B. G., Bauer, H., Bernardi, J., Bleicher, S., and Grothe, H.: Suspendable macromolecules are responsible for ice nucleation activity of birch and conifer pollen, Atmos. Chem. Phys., 12, 2541–2550, https://doi.org/10.5194/acp-12-2541-2012, 2012.

Rader, D. J. and McMurry, P. H.: Application of the Tandem Differential Mobility Analyzer to studies of droplet growth and evaporation, J. Aerosol Sci., 17, 771–788, https://doi.org/10.1016/0021-8502(86)90031-5, 1986.

Rastak, N., Silvergren, S., Zieger, P., Wideqvist, U., Ström, J., Svenningsson, B., Maturilli, M., Tesche, M., Ekman, A. M. L., Tunved, P., and Riipinen, I.: Seasonal variation of aerosol water uptake and its impact on the direct radiative effect at Ny-Ålesund, Svalbard, Atmos. Chem. Phys., 14, 7445–7460, https://doi.org/10.5194/acp-14-7445-2014, 2014.

Rastak, N., Pajunoja, A., Navarro, J. C. A., Ma, J., Song, M., Partridge, D. G., Kirkevag, A., Leong, Y., Hu, W. W., Taylor, N. F., Lambe, A., Cerully, K., Bougiatioti, A., Liu, P., Krejci, R., Petaja, T., Percival, C., Davidovits, P., Worsnop, D. R., Ekman, A. M. L., Nenes, A., Martin, S., Jimenez, J. L., Collins, D. R., Topping, D. O., Bertram, A. K., Zuend, A., Virtanen, A., and Riipinen, I.: Microphysical explanation of the RH-dependent water affinity of biogenic organic aerosol and its importance for climate, Geophys. Res. Lett., 44, 5167–5177, https://doi.org/10.1002/2017gl073056, 2017.

Reinmuth-Selzle, K., Ackaert, C., Kampf, C. J., Samonig, M., Shiraiwa, M., Kofler, S., Yang, H., Gadermaier, G., Brandstetter, H., Huber, C. G., Duschl, A., Oostingh, G. J., and Pöschl, U.: Nitration of the birch pollen allergen Bet v 1.0101: Efficiency and site-selectivity of liquid and gaseous nitrating agents, J. Proteome Res., 13, 1570-1577, https://doi.org/10.1021/pr401078h, 2014.

Reinmuth-Selzle, K., Kampf, C. J., Lucas, K., Lang-Yona, N., Fröhlich-Nowoisky, J., Shiraiwa, M., Lakey, P. S. J., Lai, S., Liu, F., Kunert, A. T., Ziegler, K., Shen, F., Sgarbanti, R., Weber, B., Bellinghausen, I., Saloga, J., Weller, M. G., Duschl, A., Schuppan, D., and Pöschl, U.: Air pollution and climate change effects on allergies in the anthropocene: Abundance, interaction, and modification of allergens and adjuvants, Environ. Sci. Technol., 51, 4119-4141, https://doi.org/10.1021/acs.est.6b04908, 2017.

Renbaum-Wolff, L., Song, M., Marcolli, C., Zhang, Y., Liu, P. F., Grayson, J. W., Geiger, F. M., Martin, S. T., and Bertram, A. K.: Observations and implications of liquid-liquid phase separation at high relative humidities in secondary organic material produced by α-pinene ozonolysis without

inorganic salts, Atmos. Chem. Phys., 16, 7969–7979, https://doi.org/10.5194/acp-16-7969-2016, 2016.

Rose, D., Gunthe, S. S., Mikhailov, E., Frank, G. P., Dusek, U., Andreae, M. O., and Pöschl, U.: Calibration and measurement uncertainties of a continuous-flow cloud condensation nuclei counter (DMT-CCNC): CCN activation of ammonium sulfate and sodium chloride aerosol particles in theory and experiment, Atmos. Chem. Phys., 8, 1153–1179, https://doi.org/10.5194/acp-8-1153-2008, 2008.

Rose, D., Nowak, A., Achtert, P., Wiedensohler, A., Hu, M., Shao, M., Zhang, Y., Andreae, M. O., and Pöschl, U.: Cloud condensation nuclei in polluted air and biomass burning smoke near the mega-city Guangzhou, China – Part 1: Size-resolved measurements and implications for the modeling of aerosol particle hygroscopicity and CCN activity, Atmos. Chem. Phys., 10, 3365–3383, https://doi.org/10.5194/acp-10-3365-2010, 2010.

Roulston, T. H., Cane, J. H., and Buchman, S. L.: What governs protein content of pollen: pollinator preferences, pollen–pistil interactions, or phylogeny? Ecol. Monogr., 70, 617-643, https://doi.org/10.1890/0012-9615(2000)070[0617:WGPCOP]2.0.CO;2, 2000.

Ruehl, C. R., Davies, J. F., and Wilson, K. R.: An interfacial mechanism for cloud droplet formation on organic aerosols, Science, 351, 1447-1450, https://doi.org/10.1126/science.aad4889, 2016.

Schneider, J., Freutel, F., Zorn, S. R., Chen, Q., Farmer, D. K., Jimenez, J. L., Martin, S. T., Artaxo, P., Wiedensohler, A., and Borrmann, S.: Mass-spectrometric identification of primary biological particle markers and application to pristine submicron aerosol measurements in Amazonia, Atmos. Chem. Phys., 11, 11415–11429, https://doi.org/10.5194/acp-11-11415-2011, 2011.

Shiraiwa, M., Ammann, M., Koop., T., and Pöschl, U.: Gas uptake and chemical aging of semisolid organic aerosol particles, P. Natl. Acad. Sci. USA, 108, 11002–11008, 2011.

Simoneit, B. R., Cardoso, J. N., and Robinson, N.: An assessment of the origin and composition of higher molecular weight organic matter in aerosols over Amazonia, Chemosphere, 21(10-11), 1285-1301, https://doi.org/10.1016/0045-6535(90)90145-J, 1990.

Sofiev, M., Siljamo, P., Ranta, H., and Rantio-Lehtimaki, A.: Towards numerical forecasting of long-range air transport of birch pollen: theoretical considerations and a feasibility study, Int. J. Biometeorol., 50, 392–402, https://doi.org/10.1007/s00484-006-0027-x, 2006.

Song, M., Marcolli, C., Krieger, U. K., Zuend, A., and Peter, T.: Liquid-liquid phase separation and morphology of internally mixed dicarboxylic acids/ammonium sulfate/water particles, Atmos. Chem. Phys., 12, 2691–2712, https://doi.org/10.5194/acp-12-2691-2012, 2012.

Song, M., Liu, P., Martin, S. T., and Bertram, A. K.: Liquid–liquid phase separation in particles containing secondary organic material free of inorganic salts, Atmos. Chem. Phys., 17, 11261–11271, https://doi.org/10.5194/acp-17-11261-2017, 2017a.

Song, T., Wang, S., Zhang, Y., Song, J., Liu, F., Fu, P., Shiraiwa, M., Xie, Z., Yue, D., Zhong, L., Zheng, J., and Lai, S.: Proteins and amino acids in fine particulate matter in rural Guangzhou, Southern China: seasonal cycles, sources, and atmospheric processes, Environ. Sci. Technol., 51, 12, 6773–6781, https://doi.org/10.1021/acs.est.7b00987, 2017b.

Stanley, R.G., and Linskens, H.F.: Pollen: Biology, Biochemistry and Management, Springer, Berlin, Heidelberg, 307 p., 1974.

Steiner, A. L., Brooks, S. D., Deng, C., Thornton, D. C. O., Pendleton,M. W., and Bryant, V.: Pollen as atmospheric cloud condensation nuclei. Geophys. Res. Lett., 42, 3596–3602. https://doi.org/10.1002/2015GL064060, 2015.

Suphioglu, C.: Thunderstorm asthma due to grass pollen. Int. Arch. Allergy Immunol., 116, 253–260, https://doi.org/10.1159/000023953, 1998.

Swietlicki, E., Hansson, H.-C., Hämeri, K., Svenningsson, B., Massling, A., McFiggans, G., McMurry, P. H., Petäjä, T., Tunved, P., Gysel, M., Topping, D., Weingartner, E., Baltensperger, U., Rissler, J., Wiedensohler, A., and Kulmala M.: Hygroscopic properties of submicrometer atmospheric aerosol particles measured with H-TDMA instruments in various environments – a review, Tellus, 60B, 432–469, https://doi.org/10.1111/j.1600-0889.2008.00350.x, 2008.

Tang, M., Gu, W., Ma, Q., Li, Y. J., Zhong, C., Li, S., Yin, X., Huang, R.-J., He, H., and Wang, X.: Water adsorption and hygroscopic growth of six anemophilous pollen species: the effect of temperature, Atmos. Chem. Phys., 19, 2247–2258, https://doi.org/10.5194/acp-19-2247-2019, 2019.

Taylor, P. E., Flagan, R., Valenta, R., and Glovsky, M. M.: Release of allergens in respirable aerosols: A link between grass pollen and asthma, J. Allergy Clin. Immunol., 109, 51–56, https://doi.org/10.1067/mai.2002.120759, 2002.

Taylor, P. E.: Thunderstorm Asthma, Curr. Allergy Asthma Rep., 4, 409-413, https://doi.org/10.1007/s11882-004-0092-3, 2004.

Trainor K., Broom, A., and Meiering, E. M.: Exploring the relationships between protein sequence, structure and solubility, 42, 136-146, https://doi.org/10.1016/j.sbi.2017.01.004, 2017.

Visez, N., Chassard, G., Azarkan, N., Naas, O., Sénéchal, H., Sutra, J.-P., Poncet, P., and Choël, M.: Wind-induced mechanical rupture of birch pollen: Potential implications for allergen dispersal, J. Aerosol Sci., 89, 77-84, https://doi.org/10.1016/j.jaerosci.2015.07.005, 2015.

von Blohn, N., Mitra, S. K., Diehl, K., and Borrmann, S.: The ice nucleating ability of pollen: Part III: New laboratory studies in immersion and contact freezing modes including more pollen types, Atmos. Res., 78, 182–189, https://doi.org/10.1016/j.atmosres.2005.03.008, 2005.

Whitehead, J. D., Irwin, M., Allan, J. D., Good, N., and McFiggan, G.: A meta-analysis of particle water uptake reconciliation studies, Atmos. Chem. Phys., 14, 11833–11841, https://doi.org/10.5194/acp-14-11833-2014, 2014.

Williams, C. G. and Després, V.: Northern Hemisphere forests at temperate and boreal latitudes are substantial pollen contributors to atmospheric bioaerosols, 401, 197-191, http://dx.doi.org/10.1016/j.foreco.2017.06.040, 2017.

Wozniak, M. C., Solmon, F., and Steiner, A. L.: Pollen rupture and its impact on precipitation in clean continental conditions. Geophys. Res. Lett., 45, 7156–7164. https://doi.org/10.1029/2018GL077692, 2018.

Xu, Y., Xiao, H., Wu, D., and Long, C.: Abiotic and Biological Degradation of Atmospheric Proteinaceous Matter Can Contribute Significantly to Dissolved Amino Acids in Wet Deposition, Environ. Sci. Technol., 54, 6551−6561, https://doi.org/10.1021/acs.est.0c00421, 2020.

Yair, Y., Yair, Y., Rubin, B., Confino-Cohen, R., Rosman, Y., Shachar, E., and Rottem, M.: First reported case of thunderstorm asthma in Israel, Nat. Hazards Earth Syst. Sci., 19, 2715–2725, https://doi.org/10.5194/nhess-19-2715-2019, 2019.

You, Y., Smith, M. L., Song, M., Martin, S. T., and Bertram, A. K.: Liquid–liquid phase separation in atmospherically relevant particles consisting of organic species and inorganic salts, Int. Rev. Phys. Chem., 33, 43-77, https://doi.org/10.1080/0144235X.2014.890786, 2014.

Zapadka, K. L., Becher, F. J., Comes dos Santos, A. L., and Jackson S. E.: Factors affecting the physical stability (aggregation) of peptide therapeutics, Interface Focus, 7, 20170030, http://dx.doi.org/10.1098/rsfs.2017.0030, 2017.

Zhang, Q. and Anastasio, C.: Free and combined amino compounds in atmospheric fine particles (PM2.5) and fog waters from Northern California, 37, 2247-2258, https://doi.org/10.1016/S1352-2310(03)00127-4, 2003.

Zhao, D. F., Buchholz, A., Kortner, B., Schlag, P., Rubach, F., Kiendler-Scharr, A., Tillmann, R., Wahner, A., Watne, A. K., Hallquist, M., Flores, J. M., Rudich, Y., Kristensen, K., Glasius, M., Kourtchev, I., Kalberer, M., and Mentel, Th. F.: Cloud condensation nuclei activity, droplet growth kinetics, and hygroscopicity of biogenic and anthropogenic secondary organic aerosol (SOA), Atmos. Chem. Phys., 16, 1105–1121, https://doi.org/10.5194/acp-16-1105-2016, 2016.

Zieger, P., Fierz-Schmidhauser, R., Weingartner, E., and Baltensperger, U.: Effects of relative humidity on aerosol light scattering: results from different European sites, Atmos. Chem. Phys., 13, 10609–10631, https://doi.org/10.5194/acp-13-10609-2013, 2013.

Zuend, A. and Seinfeld, J. H.: Modeling the gas-particle partitioning of secondary organic aerosol: the importance of liquid-liquid phase separation, Atmos. Chem. Phys., 12, 3857–3882, https://doi.org/10.5194/acp-12-3857-2012, 2012.